Unveiling Etna volcano flank dynamics from new paleoseismological findings along the Fiandaca Fault

Giorgio Tringali[1], Domenico Bella[2], Franz Livio[1], Anna Maria Blumetti[3], Gianluca Groppelli[4], Luca Guerrieri[3], Marco Neri[, 5], Vincenzo Adorno[6], Rosario Pettinato[2], Sara Trotta[1], Alessandro M. Michetti[1, 7]

[1]Dipartimento di Scienza e Alta Tecnologia, Università degli Studi dell'Insubria, Como, Italy
[2]Registered Geologist, Acireale, Italy
[3]Istituto Superiore per la Protezione e la Ricerca Ambientale (ISPRA), Roma, Italy
[4]Consiglio Nazionale delle Ricerche (CNR), Istituto di Geologia Ambientale e Geoingegneria (IGAG), Milano, Italy
[5]Istituto Nazionale di Geofisica e Vulcanologia (INGV), Osservatorio Etneo, Catania, Italy
[6]Registered Geologist, Zafferana Etnea, Italy
[7]Istituto Nazionale di Geofisica e Vulcanologia (INGV), Osservatorio Vesuviano, Napoli, Italy

Correspondence to: Giorgio Tringali (giorgio.tringali@uninsubria.it)

Abstract. We present the first paleoseismological results along the Fiandaca Fault, the source of the 26 December 2018, Mw 4.9 Fleri earthquake. We excavated two exploratory trenches along the coseismic surface ruptures at the Collegio Fiandaca site. Analysis of trench walls allow identifying, besides the 2018 event, two historical surface faulting events. The youngest one occurred in the period 1281-1926 CE, and most likely during the 1894 Fiandaca earthquake. The oldest one, previously unknown, occurred in the Early Middle Ages (757-894 CE). This paleoseismic evidence strongly suggest increased seismic activity along the Fiandaca Fault in the last centuries. In order to verify this hypothesis, we conducted detailed morphotectonic analyses and throw rate measurements along the Fiandaca and other capable normal faults in the Mt. Etna eastern flank. Throw rates mean values show an increase from 1.4 mm/yr during the 15-3.9 ka time interval to 3.4 mm/yr between 3.9 ka and the Greek-Roman period, with a further increase since the late Middle Ages, reaching 10 mm/yr. This trend suggests a very recent growth in flank instability, in agreement with current geodetic data but also with historical eruptive activity. These findings highlight an increase of the associated geological hazards along the inhabited eastern flank, emphasizing the need for further research and a multi-hazard approach to risk assessment and land planning for Mt. Etna and similar volcanic regions.

1 Introduction

Paleoseismology is a vital tool for the study of earthquake hazard and active tectonics. Nonetheless, its application in the context of Late Quaternary basaltic volcanoes encounters considerable limitations due to the inherent highly dynamic nature of such systems. Etna volcano, however, provides an ideal setting for overcoming these limitations. In particular, the densely populated Mt. Etna eastern flank records frequent surface faulting earthquakes and aseismic fault creep, which result in significant offsets of well-dated historical landforms and stratigraphy, including lava flows, interlayered pyroclastic deposits, and anthropic structures. This allows for the analysis of paleoseismic events and fault slip rates across various time scales

(Monaco et al., 1997; Azzaro et al., 2000; Ferreli et al., 2002). Not much has been done since the first paleoseismological studies in the early 2000's, but the extensive building damage and surface faulting produced by the 2018 Fleri earthquakes renewed interest in Mt. Etna capable faults characterization (Monaco et al., 2021; Azzaro et al., 2022; Tringali et al., 2023a).

35   Detailed historical earthquake records for Etna illustrates severe frequent building damage and ground ruptures. Still, they mostly date back to the second half of the 1800s, leaving sparse or even no information about earlier periods. In this framework, paleoseismology might play a crucial role for detecting earthquakes that precede the historically known ones, and to evaluate the slip rates variations over longer time windows.

Due to intense tectonic and gravitational deformation resulting in diffuse coseismic and aseismic surface faulting, Mt. Etna is

40   a natural laboratory to gain further knowledge of these geological processes (Rasà et al., 1996; Azzaro, 1999). For example, offset of well-dated landforms, lava flows and anthropic structures allows the analysis of fault slip-rates variations over different time scales, from the Late Pleistocene to the present. Therefore, Mt. Etna offers the opportunity to test methodologies to try disentangling gravitational transients from purely tectonic and volcanic-induced deformation. Moreover, the study of several volcano-tectonic events suggests that dike intrusions, eruptions, flank instabilities and surface faulting are closely

45   related each other (Acocella et al., 2003; Walter et al., 2005a; Neri et al., 2009; Mattia et al., 2015). Thus, the extensive documentation about flank eruptions allows understanding of feedback between the seismic and volcanic processes, leading to a better knowledge of the volcano behaviour.

In this paper, we provide an accurate description of the first paleoseismological results along the Fiandaca Fault (FIA in Fig. 1) and analyse its recent coseismic activity and throw rate variations over time. The 2018 post-earthquake urban reconstruction

50   work allowed us to dig two trenches in the Collegio Fiandaca site (see location in Fig. 1) to verify whether it was possible to rebuild in the same area. While post-earthquake reconstruction may present new opportunities for research, it has not been possible to excavate along the entire fault zone due to logistic constraints and requests of landowners. However, the location of the trench in the central portion of the Fiandaca Fault and the significant effects of the 2018 surface faulting allowed us to study the entire fault rupture. These results provided suitable information for relocating the residential buildings in the area

55   affected by coseismic scarps. Furthermore, the trenches allowed us to recognize past surface faulting events.

Based on this paleoseismic investigation, we conducted a careful analysis of the fault scarps to assess throw rates resulting from the displacement of different ages lava flows along the Fiandaca Fault and nearby extensional structures: Aci Catena, Aci Platani, San Leonardello, Santa Tecla and Trecastagni faults (CAT, PLA, LEO, TEC and 3CA in Fig. 1). A similar approach was applied along the Pernicana Fault (PER in Fig. 1a) where throw rates in acceleration were observed in the last

60   3.5 ka (D'Amato et al., 2017). We analyse the obtained throw rates in comparison with recently published morphotectonic, geodetic, seismicity and eruptive history investigations (e.g., Bencke and Neri, 2003; Bencke et al., 2005; Neri et al., 2009; Neri et al., 2011; Bonforte et al., 2011; Azzaro et al., 2012; Azzaro and D'Amico, 2014; D'Amato et al., 2017; Branca and Abate, 2019; Guidoboni et al., 2019; Bevilacqua et al. 2022; Carnemolla et al., 2023; Palano et al., 2023) to assess long and short-term fluctuations and their relations with the entire volcano flank dynamics.

65
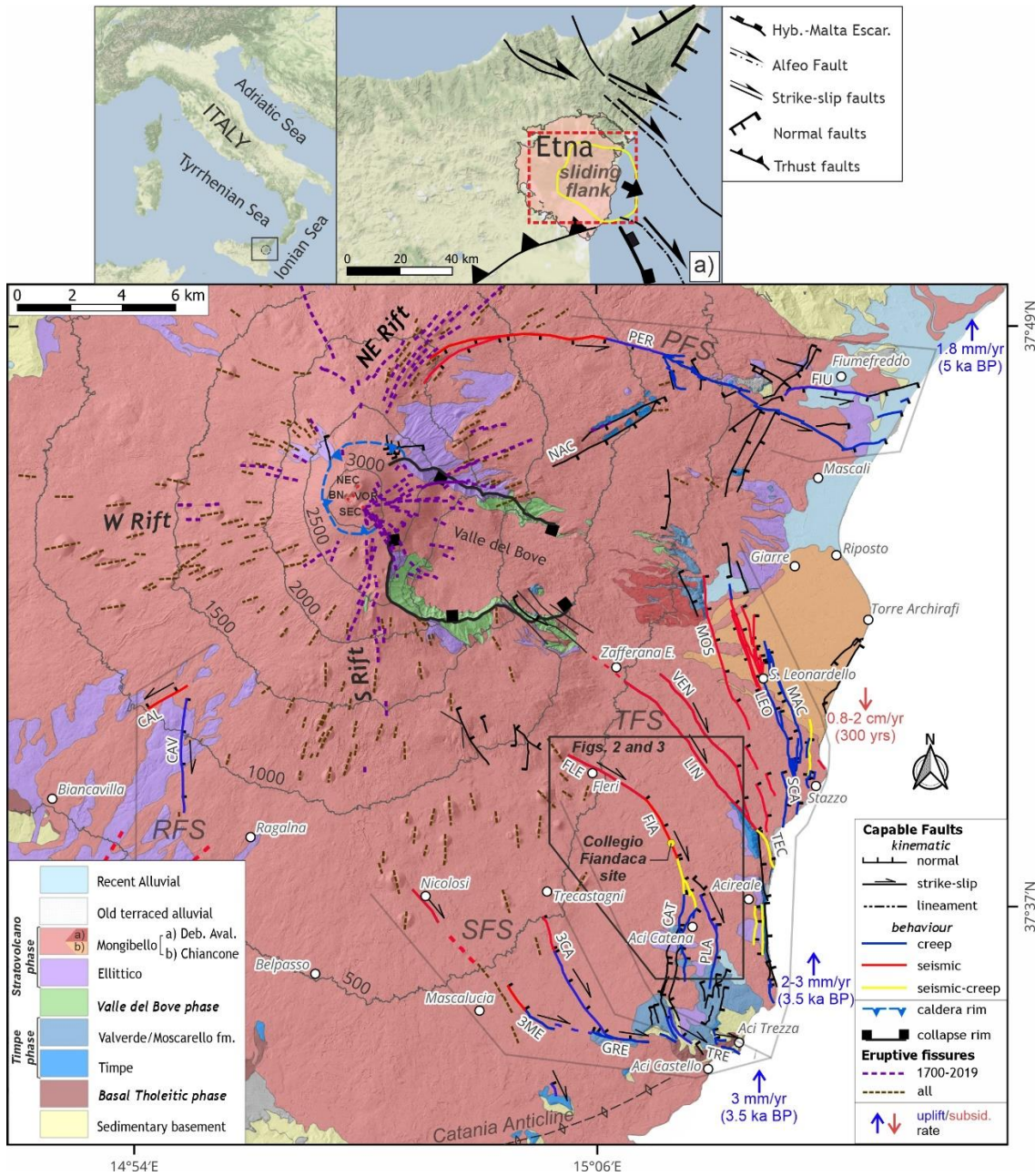
Figure 1: Simplified geological and volcano-tectonic map (modified after Branca et al., 2011a; Azzaro et al., 2012; ITHACA Working Group, 2019; Barreca et al., 2013; Bevilacqua et al., 2022; Branca et al., 2011a; Neri et al., 2011); black lines are faults and lineaments (dashed where uncertain) with their kinematics and seismic/creep behaviour, and eruptive fissures; TFS: Timpe fault system; PFS: Pernicana fault system; SFS: Southern fault system; RFS: Ragalna fault system. Faults labels: FIA: Fiandaca; FLE: Fleri; PLA: Aci Platani; CAT: Aci Catena; LIN: Linera; TEC: Santa Tecla; VEN: Santa Venerina; MOS: Moscarello; SCA: Scalo Pennisi; LEO: San Leonardello; MAC: Macchia; CAL: Calcerana; CAV: Masseria Cavaliere; 3ME: Tremestieri; 3CA: Trecastagni; GRE: San Gregorio; TRE: Aci Trezza; PER: Pernicana; FIU: Fiumefreddo; NAC: Ripe della Naca. Etna Central Craters (red dots) labels: VOR: Voragine; BN: Bocca Nuova; NEC: Northeast Crater; SEC: Southeast Crater; inset (a) shows the general tectonic framework of NE Sicily with Etna volcanic edifice and its sliding flank borders (in yellow).

2 Geological setting

2.1 Geological evolution and volcanic activity

Etna volcano has a peculiar position in the Mediterranean geodynamics, located on the Appennine-Maghrebian active fold and thrust belt (Fig 1a; Doglioni et al., 2001; Branca et al., 2011a), resulting in local uplift rates of 1-3 mm/yr estimated for the last
80   5 kyr (Branca et al., 2014). The current volcanic edifice is the result of the superimposition of different volcanoes during the last 180 ka (Branca et al., 2011a), starting with the Timpe (180-110 ka) and Valle del Bove phases (110 ka-65 ka). About 65 ka ago, the volcanic activity migrated to the W with the inception of a stratovolcano phase with two different volcanoes: Ellittico (65 ka-15 ka) and Mongibello (15 ka-present). Mt. Etna is currently one of the most active volcanoes in the world and its activity is mainly localised in the summit area with eruptive episodes in the central craters (VOR, BN, NEC and SEC in
85   Fig. 1; Acocella et al., 2016), or in subterminal monogenic craters. The eruptions are characterised by a prevalent strombolian activity with the deposition of fall out deposits and basaltic lava flows. The eruptive activity is sometimes located in the flanks along eruptive fissures, feed by dykes (i.e., lateral or flank eruptions), and interesting mostly the so-called NE, S and W Rifts (Neri et al., 2011; Azzaro et al., 2012; Tibaldi et al., 2021; see location in Fig. 1). Starting from 7478-7134 BCE (Malaguti et al., 2023), a series of catastrophic collapses along the eastern flank produced a wide depression known as Valle del Bove
90   (Guest et al., 1984; Calvari et al., 1998, 2004). The collapses are evidenced by debris avalanches deposits at the open end of the Valle del Bove (Branca et al., 2011b). They have been subsequently eroded and reworked generating, with a series of alluvial events, a wide alluvial fan along the Ionian coast locally named Chiancone (Calvari and Groppelli, 1996). Mt. Etna has probably experienced other past flank collapses as inferred by two valleys E-W elongated in the sedimentary basement (Branca and Ferrara, 2013).

95   Regarding past eruptions, during the Greek-Roman and Medieval period, the opening of eruptive fissures was common below 1400 m of elevation (Branca and Abate, 2019). These eruptions culminated with an eruptive cycle associated with high volumes of lava laterally erupted in the period 1600-1669 CE by big flank eruptions (Bencke and Neri, 2003). After the 1669 CE eruptive event there was a drastic change in the volcanic behaviour andwith the opening of fissures mainly in the upper-middle flanks between 1600 m and 2500 m a.s.l., suggesting a change in the plumbing system (Branca and Del Carlo, 2005;
100   Branca and Abate, 2019). In the last three centuries the opening of new fissures has been concentrated above 1000 m of elevation (Branca and Abate, 2019), with two long term eruptive cycle starting from 1760 and 1865 CE respectively (Bencke and Neri, 2003). The cycle started in 1865 CE is characterized by more frequent flank eruptions and higher volumes of erupted products then the previous one (Bencke and Neri, 2003). The W Rift is currently less active but produced many eruptions before the 1600 CE (Neri et al., 2011; Branca and Abate, 2019).

2.2 Seismotectonic and flank instability

The eastern and southern flanks of the Etna volcano include several capable faults characterized by coseismic and aseismic slip (Fig. 1; Borgia et al., 1992; Rasà et al., 1996; Gresta et al., 1997; Azzaro, 1999; Azzaro et al., 2012; Barreca et al., 2013).

The NE flank is affected by the Pernicana fault system (PFS in Fig. 1; Acocella and Neri, 2005) with two main fault segments (PER and FIU in Fig. 1) characterized by prevalent left-lateral kinematics, and stick-slip behaviour to the W, whereas aseismic

110   creep is dominant to the E. The Ragalna fault system (RFS in Fig. 1; Rust and Neri, 1996) affects the SW flank of the volcano with two fault segments (CAV and CAL in Fig. 1). The Etna E flank is affected by the mainly NNW-trending Timpe fault system (TFS in Fig.1) characterized by a general E-W extension along normal faults dipping toward the E, with right lateral strike-slip components (Lanzafame et al., 1996; Monaco et al., 1997). The SE flank is interested by the Southern Faults System (SFS in Fig. 1), composed of normal and right lateral strike-slip faults (Azzaro et al., 2012; Barreca et al., 2013). These

115   structures separate shallow sliding blocks (Bonforte et al., 2011; Siniscalchi et al., 2012; Acocella et al., 2013; Azzaro et al., 2013) due to gravitational collapse of the entire sector toward the Ionian Sea (Neri et al., 1991; Borgia et al., 1992; Lo Giudice and Rasà, 1992; Solaro et al., 2010; Chiocci et al., 2011; Gross et al., 2016; Urlaub et al., 2018). The boundaries of the gravitational collapse are defined by the PFS in the NE flank (Neri et al., 2004), and by the SFS and RFS in the S (Rasà et al., 1996; Rust and Neri, 1996) with deformation primarily transferred along the San Gregorio-Aci Trezza faults (GRE and TRE

120   in Fig. 1; Azzaro et al., 2013; Urlaub et al., 2018, 2022). The unstable flank is bounded in the summit area by the NE and S Rifts going through the central craters (Acocella et al., 2003, 2016). Furthermore, two ENE-WSW and NE-SW normal structures named Ripe della Naca faults (NAC in Fig. 1) are located between the PFS and the TFS. NAC are interpreted as inherited neotectonic faults of the buried basement (Azzaro et al., 2012).

The interpretation of the TFS and its driving-mechanism has been widely debated in literature. Specifically, TSF has been

125   interpreted as: i) the inland continuation of the Malta Escarpment (Lanzafame and Bousquet, 1997; Monaco et al., 1997; Neri et al., 2018); ii) part of gravitational structures affecting the offshore margin of Mt. Etna (Borgia et al., 1992; Chiocci et al., 2011; Gross et al., 2016; Urlaub et al., 2018; Murray and de Vries, 2022); iii) a secondary splay of a main dextral E-W striking shear zone (Firetto Carlino et al., 2019); iv) the northern termination onshore of the Alfeo Fault offshore (Fig. 1a; Monaco et al., 2021). Regardless the TFS meaning, these faults induce localized subsidence, interrupting the Latest Pleistocene to

130   Holocene regional uplift, with rates of 0.8-2 cm/y along the coastline between Stazzo and Torre Archirafi villages (Carveni et al., 2005). The subsidence is typically related to the gravitational sliding, as it is further demonstrated by recent geodetic data (Bonforte et al., 2011; Palano et al., 2023; Carnemolla et al., 2023).

The Etna E flank is characterized by frequent diffuse surface faulting mostly along the PFS, TFS and SFS (Rasà et al., 1996; Gresta et al., 1997; Azzaro, 1999). Moderate magnitude (Mw<5) earthquakes, with a shallow hypocentral depth, mostly less

135   than 2 km, generate coseismic surface rupture and significant damage to the urban areas (Carveni and Bella, 1994; Azzaro, 1999; Azzaro et al., 2017). Historical events reached maximum macroseismic intensity of grade VIII-IX in the EMS scale (Azzaro et al., 2017).

Aseismic creep events are common along the lower eastern flank faults, occurring during periods of seismic swarms as well as during times of low seismic activity (Rasà et al., 1996; Palano et al., 2022). Recently, several studies highlighted that most

140   of the deformation is aseismic and accommodated with frequent slip transients of acceleration occurring in the lower E flank ("Slow Slip Events"; Mattia et al., 2015; Palano et al., 2022; Carnemolla et al., 2023). The shallow deformation is concurrently

driven by volcano-tectonic and gravity processes (Rasà et al., 1996; Tibaldi and Groppelli, 2002) that can be also influenced by the sedimentary basement morphology and the thickness of the volcanic pile (Palano et al., 2022; Tringali et al., 2023a; Tringali et al., 2023b).

3 Geologic features around the Fiandaca Fault

3.1 Stratigraphic framework

The area under investigation is located on the lower SE flank, in a sector characterised by scattered dwellings and lemon trees established on historic Mongibello lava flows (Branca et al., 2011b; Fig. 2) of the Torre del Filosofo formation (volcanic products of the period 122 BCE-1669 CE) and Pietracannone formation (3.9 ka-122 BCE Upper member and 15 ka-3.9 ka Lower member). The lava flows outcropping in the area are mostly attributed to eruptions that occurred in the lower eastern flank in the period 3.9 ka – 122 BCE (Fig. 2) that were partially covered by new flows during the Medieval period (e.g., IX century AD and 1329 CE). In the trenching site the outcropping lava is the Mt. Salto del Cane (*sd* in Fig. 2) lying on a ~3000 years old paleosoil (Del Carlo et al., 2004; Branca et al., 2011b). The 122 BCE tephra fallout is a marker stratigraphic bed, due to a Plinian basaltic eruption that led to the formation of a vast pyroclastic deposit that covered the SE flank of the volcano, about 10-30 cm thick around the trenching site (Coltelli et al., 1998; Branca et al., 2011b). The onset of a new lateral eruption in 1329 CE formed the M. Rosso scoria cone, and the lava flow erupted reached the area of Santa Maria la Stella to the N of Acireale (Fig. 2). Toward the S, in the Aci Catena area, some lava flows (*ay*, *mr* and *tr* in Fig. 2) covered between 3.9 ka and 122 BCE, the 15 ka Aci Platani lava flow (*at* in Fig. 2) and the Valverde formation.
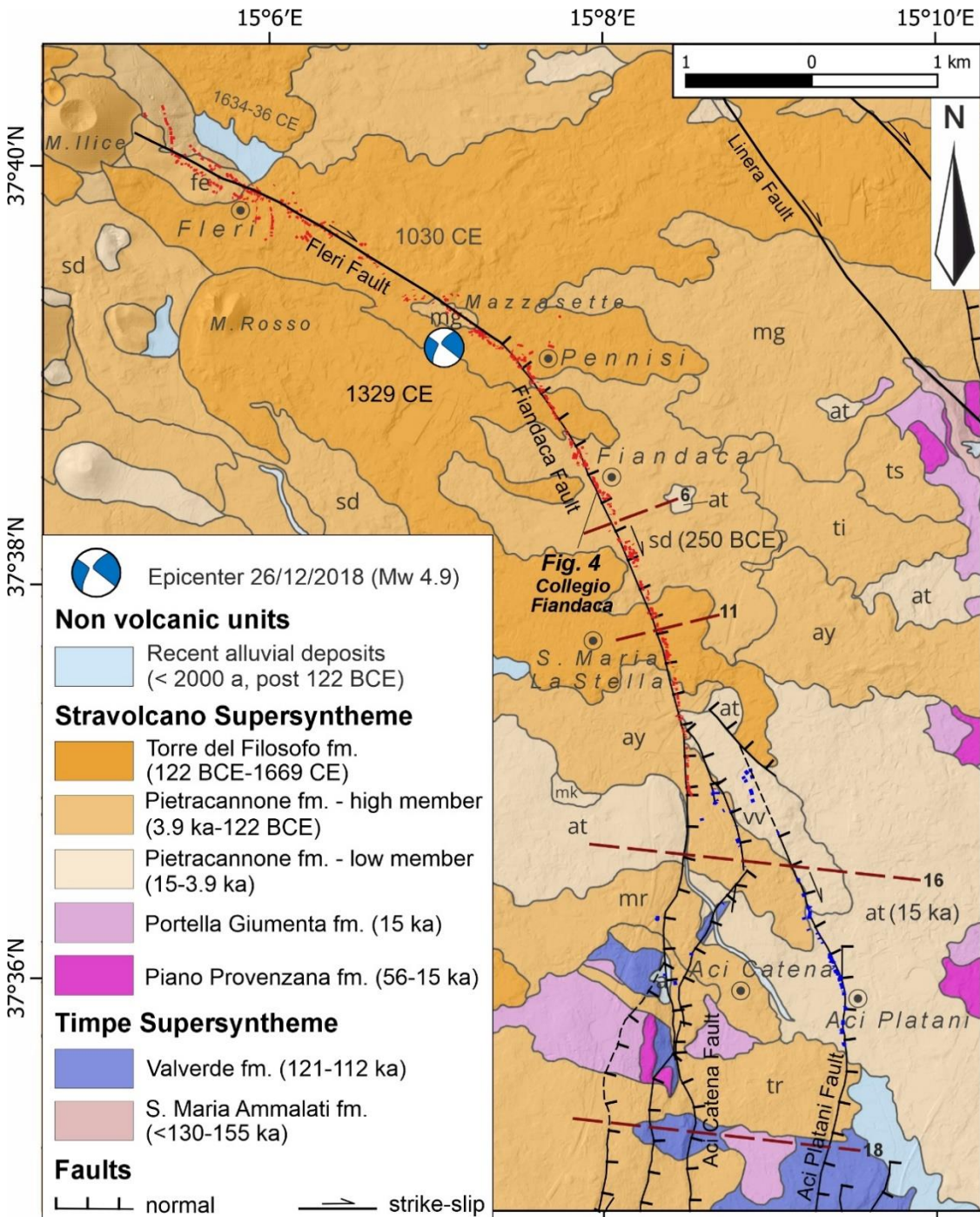
Figure 2: Geological map of Mt. Etna E flank around the Fiandaca Fault (modified after Branca et al., 2011; Azzaro et al., 2012; Barreca et al., 2013; ITHACA Working group, 2019); in red the coseismic ruptures of the 26 December 2018 earthquake, in blue the fractures related to the accompanying aseismic creep events (modified after Tringali et al., 2023a); dark red dashed lines are selected profiles across faulted lava flows (n. 6, 11, 16, 18); lava flow labels: sd: M. Salto del Cane; mr: M. Serra; tr: Trecastagni; fe: Fleri; mg: M. Gorna; ay: Piano d'Api; mk: Monaci; vv: Villa Vincenzina; at: Aci Platani.

3.2 Morphotectonic and historical seismicity

The Fiandaca Fault (FIA) is part of the TFS and stretches for an overall length of ~4.5 km from Pennisi to the N of Aci Catena with a curvilinear, almost NNW-trending trace (Fig. 2). From the kinematic point of view, FIA is a normal fault with a right-lateral slip component. Small but evident degraded scarps, typically less than 10 m high, reflecting long-term vertical displacement, mark the fault trace. At its N termination, FIA directly connects to the NW-striking Fleri Fault (FLE), while to the S it connects directly to the Aci Catena Fault (CAT) and, through several fault splays and multiple parallel scarps, to the Aci Platani Fault (PLA). CAT shows multiple fault strands with mostly a N-trending, displacing with a normal component Mongibello lavas and to the S also 115 ka lava flows of the Valverde formation (Branca et al., 2011a). CAT is characterized by retreated, up to 70 m high, fault scarps. Two of them intersect the 115 ka lavas, resulting in a cumulated vertical offset of ~90 m. To the S, CAT changes its strike to NNW-SSE and NW-SE connecting to the E-W Aci Trezza Fault (TRE in Fig.1). PLA has a curvilinear trace with strike changing from NNW-SSE to NNE-SSW (Fig. 2) with 5 to 20 m high scarps.

FIA is one of the most active faults of TFS, characterized by a significant seismic activity (Fig. 3). The trenching site is in the central sector of FIA, where only coseismic fault activation has been documented over the last 150 years. This sector is characterized by well evident surface ruptures with vertical displacement occurred during at least 9 earthquakes in the last 600 yr (Fig. 3; see Supplementary Table S1; Azzaro, 1999; Tringali et al., 2023a). The first known strong earthquake occurred during the seismic swarm that preceded and accompanied the 1329 lateral eruption (Guidoboni et al., 2019). Nevertheless, there is no clear information about earthquakes and associated surface ruptures between 1329 and 1600 CE. Azzaro and Castelli (2015) revised the historical sources during the period 1600-1831 CE, recognizing at least 6 earthquakes that could be associated with the TFS (see Appendix A and Table A1), one of them occurred in April 1809 is associated with ground ruptures but without a precise location. Despite the uncertainties, the highly felt earthquakes in Acireale and Zafferana Etnea strongly suggest a causative fault identified in FIA or LIN, as these faults are closest to the affected villages (see Fig. 1a). In spite the FIA high seismic activity, its S termination shows also slow and constant aseismic creep as testified by the frequent damage along buildings, roads and walls crossed by the fault.

CAT and PLA have recently experienced frequent aseismic creep phenomena (see Supplementary Table S2) showing a maximum short term throw rate of 2.3-6 mm/yr for CAT in the period 1970-2000 (Rasà et al., 1996; Bonforte et al., 2011). In particular, the last aseismic creep episodes with surface faulting occurred in 2023 along CAT (Tringali, 2023) and in 2018 along PLA (Tringali et al., 2023a).
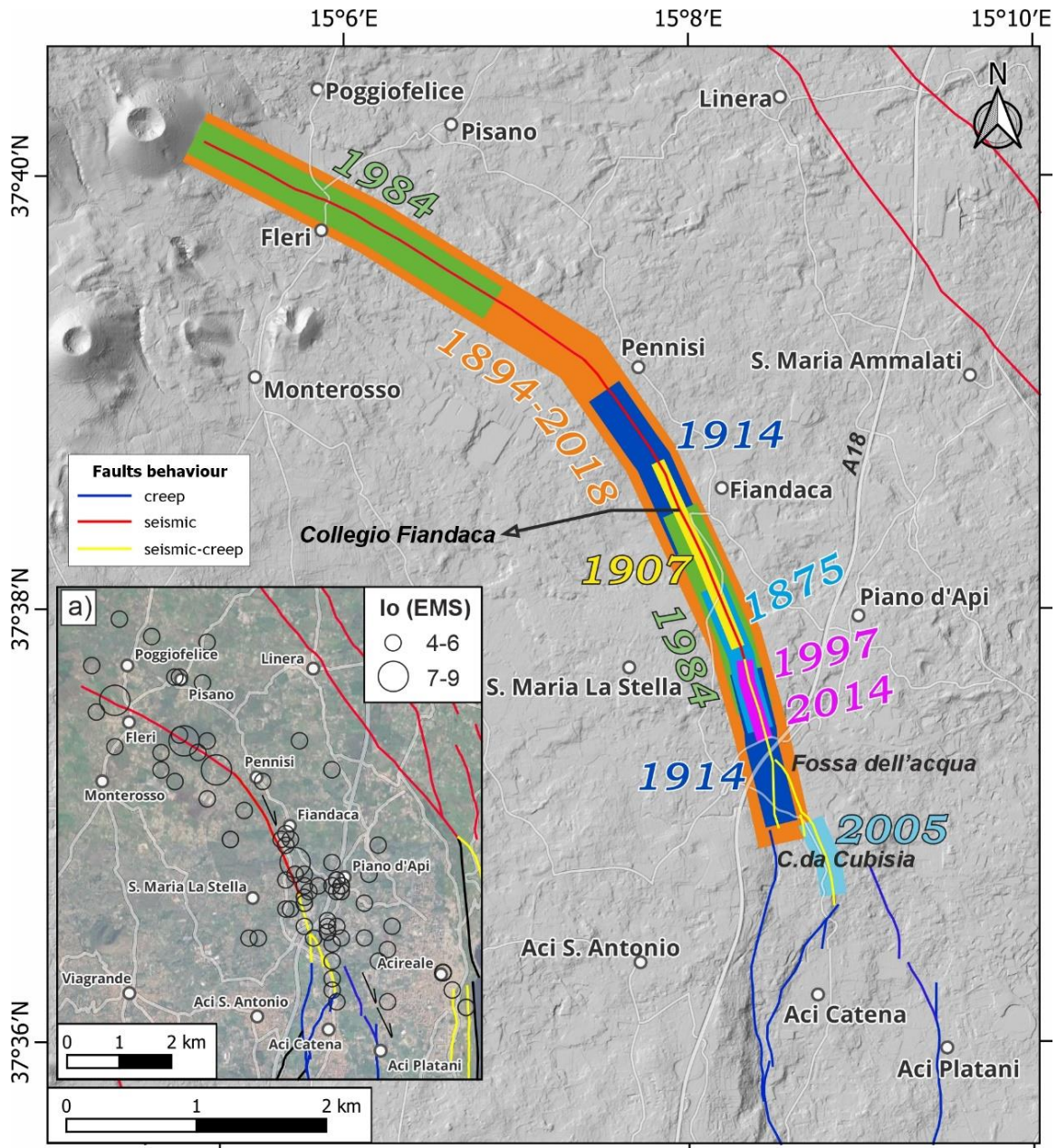
Figure 3: Map showing 1875 CE to present surface faulting events along the Fiandaca Fault, coloured segments represent the earthquake ruptures. In the inset (b) the seismicity around the Fiandaca Fault from 1633 CE, Io is the epicentral intensity (after Azzaro and D'Amico, 2014).

3.1.1 26 December 2018 surface faulting

The 26 December 2018 Fleri earthquake (M_L 4.8 – M_w 4.9; Bonforte et al., 2019; De Novellis et al., 2019) generated 8 km of surface faulting along FIA and FLE (Civico et al., 2019; Tringali et al., 2023a). The ruptures showed a clear en-échelon pattern along FIA with left-stepping transtensive fault grabens. The maximum observed throw is 45-50 cm along the central sector of FIA with a general increase moving to the S (Azzaro et al., 2022; Tringali et al., 2023a). The heave values were particularly high in some localities, up to 120 cm, due to graben collapses and the formation of deep and elongated sinkholes.
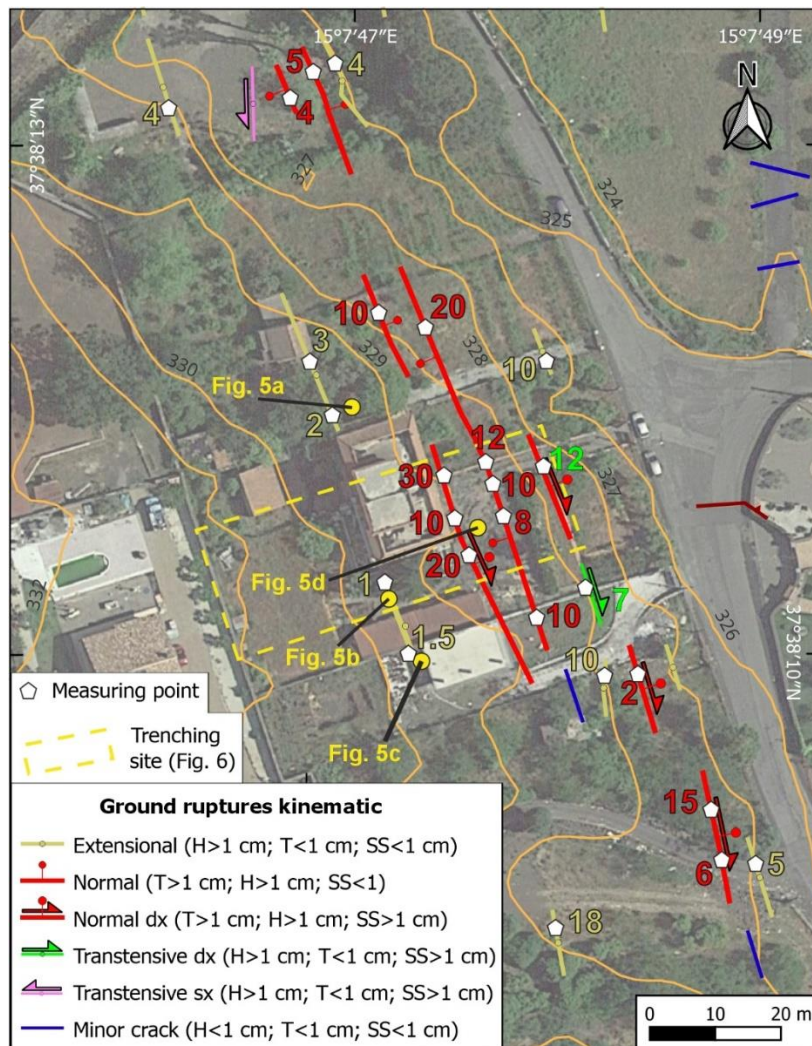
Figure 4: December 26, 2018, earthquake ground ruptures map at the Collegio Fiandaca site (modified after Tringali et al., 2023a); numbers show the amount of heave (H, in yellow), throw (T, in red) and strike-slip (SS, in green); yellow dots are field photos location of Fig. 5.

210   At Collegio Fiandaca site we observed four ground ruptures striking N150-170° (Fig. 4). The ruptures reactivated a pre-existing, ~8 m high, degraded fault scarp. The W-most ruptures are quite discontinuous small open cracks with a 0.5-2 cm heave, offsetting pavements and walls of the buildings over a length of ~10 m (Figs. 4, 5b and 5c). The E-most rupture displaced the asphalt and the walls, showing a transtensive kinematic with up to 3 cm heave and 2 cm throw, and a prevalent right lateral offset of 12 cm (Fig. 4). The central part of the fault zone showed two main ruptures delimiting a 4-5 m wide and more than

215   10 m long graben (Figs. 4 and 5d). The main fault of the graben showed up to 30 cm throw (with an average of 20 cm), up to 15 cm heave, and 4 cm right-lateral offset. The antithetic fault showed a maximum heave and throw of 12 cm with an average of 10 cm.

220   **Figure 5: 26 December 2018 coseismic ruptures at Collegio Fiandaca trench site (see photos location in Fig. 4): a) ground rupture along a private road with few cm of offset; b) ground rupture which follows a damaged building wall, offset ~1 cm; c) 1.5 cm horizontal offset between two floor tiles continuing into the wall; d) fault graben on a private asphalt parking which extends over the wall and farmland.**

4 Methods and materials

4.1 Paleoseismology, trenching, logging and sample dating

We excavated two trenches, coded as FIA1 and FIA2 (see location in Fig. 6), across the 2018 coseismic ruptures to a maximum depth of 3 m (see Table 1 for details). We meticulously cleaned the trench walls in order to facilitate accurate recognition of natural stratigraphy. Parts of the trenches encountered thick anthropic refill and therefore were not cleaned and studied. It was possible to study the natural stratigraphic and tectonic features along the trench sections named N-Wall, S-Wall1 and S-Wall2, for the FIA1; and N-Wall, for the FIA2. We identified the main stratigraphic units and the faults based on the deposit grain-size distribution, fabric and colour, separated by bed tops of unconformities, considered as horizons. Horizons were flagged with coloured pins and logged. We logged the trench walls at 1:50 scale. We used UAV survey to obtain a detailed orthophoto image of the trench site. We generated three ortho-photomosaics from a 3D digital model of the trench walls, obtained by the processing of ground-based 24-megapixel imagery means of common Structure-from-Motion photogrammetry workflow (Agisoft Metashape® software). These new technical and instrumental developments in paleoseismic studies allow better characterization of a fault zone (McCalpin et al., 2023).

Table 1: Features of the FIA1 and FIA2 paleoseismological trenches.

Trench	Realization	Trending	Length	Max depth
FIA1	6-13 February 2023	N75°	40 m	3 m
FIA2	13-17 February 2023	N75°	11 m	2 m

We collected three charcoal samples and subsequently dated by AMS at CEDAD (CEntro di DAtazione e Diagnostica, University of Salento). For the determination of the experimental error in the radiocarbon date, the scattering of the data around the mean value and the statistical error resulting from the ^{14}C count were considered. We collected one sample of tephra in FIA2 that was analysed in the INGV-OE labs by Mauro Coltelli. Two additional samples (EFIA and WFIA) were collected in the easternmost and westernmost part of FIA1 to assess chemical analysis for a better constrain of the recognized horizons (see further information in Supplementary Material).

4.2 Field survey and seismic tomography

We conducted a two-month field survey following the December 26, 2018, earthquake, starting in the night of the mainshock (see Tringali et al., 2023a). In particular, we conducted field surveys at the Collegio Fiandaca trenching site on 29 and 31 December 2018; 22 January 2019; and February 18, 2019. Before trenching, we performed a seismic refraction tomography survey, in order to investigate the subsurface fault zone width. The instrumentation used for the survey consists of a 24 channel seismograph (MAE sysmatrack), 2 seismic cables with 12 sockets each, 13 geophones with a frequency of 4.5 Hz and one 8 kg hammer. To enhance the definition of the underground seismic refractors, we used seven energization points during the tomography data acquisitions. We processed seismic data using SeisOpt® @2D software.

4.3 Evaluation of throw rates

The throw values have been estimated from geological profiles where the lowest anthropic disturbance occurred (i.e., low
255 presence of buildings) and forest coverage. The profiles were realized only where the thickness of the lava flows was more
than 10 m, to be sure of measuring actual and not inherited throw values from previous scarps.

All the profiles, with associated fault throw and throw rates, and their locations are available in the supplementary materials.
The throw rates obtained have been compared with others published recently.

The DTM (https://www.sitr.regione.sicilia.it/geoportale/it/Metadata/Details/946) used to realize the topographic profiles and
260 to estimate the lava flows thickness has generally an accuracy of ±0.3 m increasing at ±0.6 m in areas covered for the 70% by
tree vegetation. Therefore, the calculated throws have an accuracy of ±0.3 m.

5 Trenching site results

5.1 Trench stratigraphy and seismic tomography

The paleoseismological trench FIA1 and FIA2 were oriented N75° across the 2018 coseismic ruptures (Fig. 6a), enabling
265 assessment of the width of the deformation zone, and identification of pre-2018 displacement events. We excavated FIA2 at
the E termination of the FIA1, extending the initial trench to better investigate the fault zone in the sector affected by the
hanging wall graben.
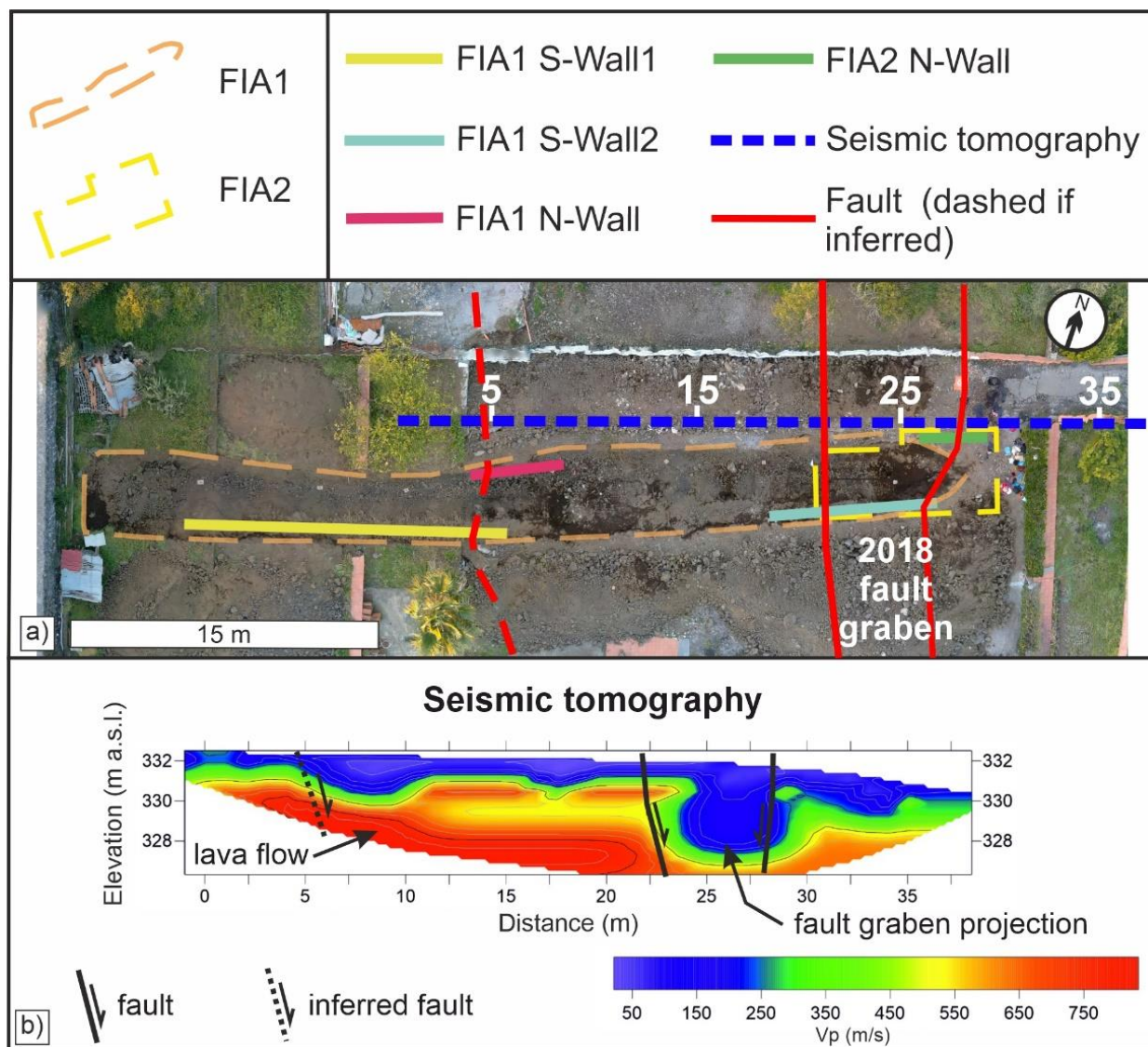
Figure 6: Map of Collegio Fiandaca trench site: a) orthophoto mosaic obtained by aerial drone photos showing FIA1 and FIA2 with sectors of the walls investigated in detail, and faults in accordance with the 2018 coseismic ruptures; dashed blue line is the trace of seismic tomography showed in (b).

The accurate analysis of the two trenches allowed us to identify three stratigraphic units lying on volcanic blocks associated to the top of the M. Salto del Cane lava flow (*sd* in Fig. 2), commonly outcropping in the area. The stratigraphic units are covered by reworked anthropogenic material, in some cases directly overlapping the *sd* lava flow. The units are synthesised and described in Table 2.

280 **Table 2: Stratigraphic units identified along the FIA1 and FIA2 walls.**

Unit Code	Description
sd lava flow	Volcanic scoria and breccia and isolated hard basaltic rock belonging to the *sd* lava flow
U1	Pyroclastic deposit significantly reworked characterized by high vesiculated, millimetric to 1 cm lapilli with tabular plagioclase crystals.
U2	Deposit characterized by loose medium sands with minor silt and rare subrounded millimetric to 5 cm clasts and rare fragments of historical bricks, the base of the deposit is reddish (7,5YR/3R) passing upwards to a dark brown colour (5YR 3/2).
U3	Deposit characterized by loose medium sands with minor silt and rare subrounded mm to cm clasts, roots, fragments of historical bricks and embedded remains of U1. The colour is black (5YR 2,5/1).
R1/R2	Anthropic reworked deposit characterized by medium dark brown sands with lava blocks, recent bricks fragments and plastic. R2 has a higher lava blocks content, in the FIA1 N-Wall and is a dig refilling crosscutting R1.

U1 is missed in many parts of the trenches, especially in the western side. An erosive surface recognized in both trenches separates U2 and U3. The seismic tomography in Fig. 6b shows two main seismic layers with different Vp values. The shallowest layer, indicated in blue, can be ascribed to the U1, U2 and U3 identified within the trench. The second layer with

285 higher Vp is attributed to the *sd* lava flow observed at the base of the trenches (Fig. 6b), which exhibits a minimum vertical displacement of ~3 m. The low-velocity zone between the progressives 22-28 m can be associated with the main damaged fault zone of FIA that corresponds to the surface fault graben (Fig. 6b).

5.1.1 Units dating

Radiocarbon dating for 3 collected samples was calibrated and the result of the calibration is shown in Table 3.

290 **Table 3: Calibrated dating of the charcoal samples collected in the FIA1 and FIA2 trenches.**

Trench	Unit code	Sample code	Lab code	Calibrated Dating (confidence level 2σ)
FIA1	U2	S1	LTL31802	677AD (21.3%) 749AD 757AD (72.2%) 894AD 928AD (2.0%) 945AD
FIA1	U3	S2	LTL31803	1687AD (26.6%) 1731AD 1806AD (68.8%) 1926AD
FIA2	U3	S3	LTL31801	1281AD (95.4%) 1400AD

The *sd* lava flow at the bottom of the trench has an archaeomagnetic age of 150±200 BCE (Tanguy et al., 2012). The pyroclastic deposit U1 can be ascribed to the 122 BCE (personal communication by Mauro Coltelli) aligning with its petrographic features described by Coltelli et al. (1998). Meanwhile U2 and U3 are identified as a colluvial deposit. U2 dates to the early medieval period in accordance with S1 radiocarbon dating. U3 may be likely from the late medieval period to the beginning of the last century, based on radiocarbon dating of S2 and S3.

5.2 FIA1 trench

For the FIA1 trench, 3 separated logs were realized named: N-Wall, S-Wall1, S-Wall2.

In the western portion of FIA1 S-Wall1, the stratigraphy is sub-horizontal with U2 directly covering *sd* in most of the section (Fig. 7a and b). Toward the east from 5 m to 0 m along section, the beds, including the sd roof, are tilted to a dip of 10° angle, increasing eastward to 15°, starting from 12 m (Fig. 7a and b). This part of the trench is characterized by an apparent thickening of the colluvium of unit U2 and the progressive increase of the eastward dipping angle of the units (Fig. 7b), which could be ascribed to an inferred fault activity. The inferred fault displaces U2 of about 20 cm.

The FIA1 N-Wall (Fig. 7c and d) shows an eastward dipping fault plane that displaces the base of U2 and the top of *sd* showing a vertical offset of about 40 cm. The original roof of U2 and part of *sd* top have been eroded by two anthropogenic excavations filled with R1 and R2 (Fig. 7d), hence the clear evidence of surface faulting may have been removed. The thickness of U1 is apparently greater on the hanging wall of the fault (Fig. 7d) suggesting a colluvial deposition during the tectonic processes. The faults observed in S-Wall1 and N-Wall of FIA1 are uncertain due to the erosive surface that truncates U2 (Fig. 7).
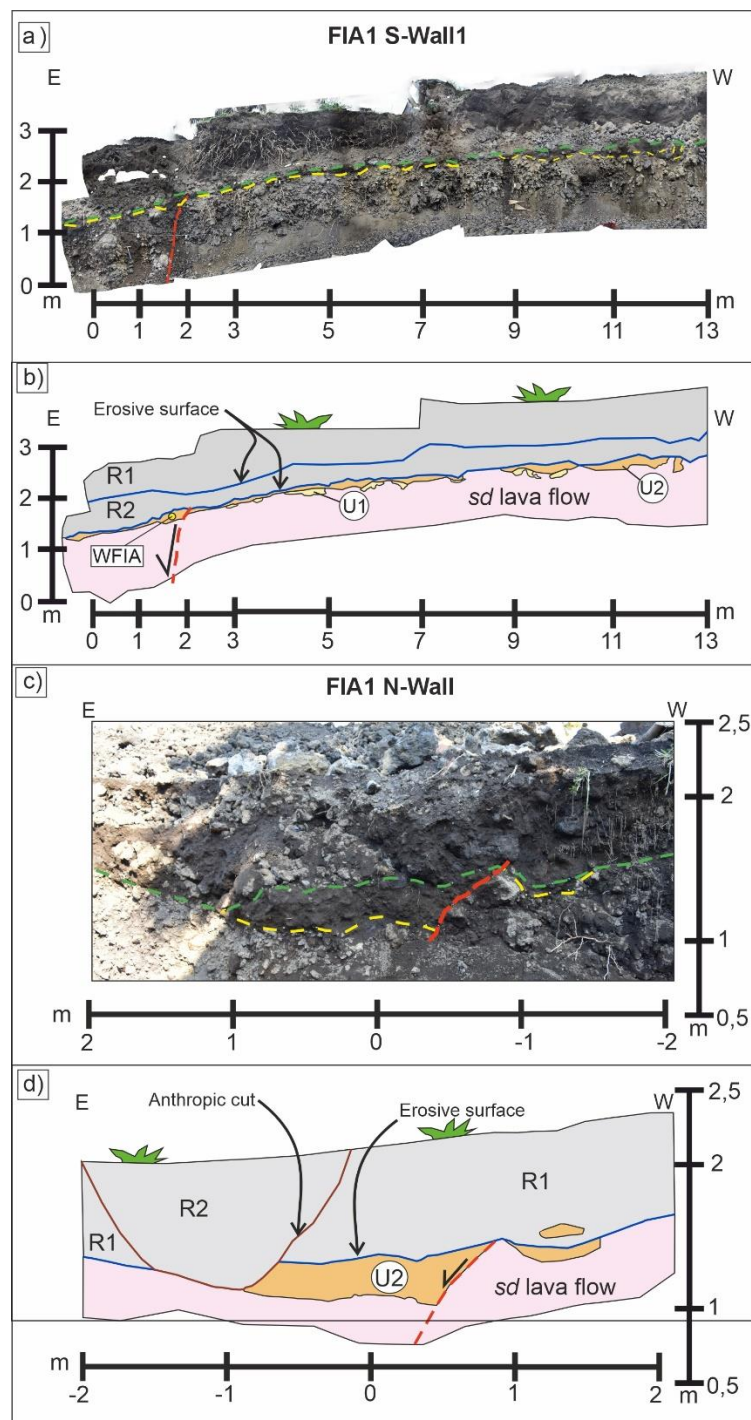
Figure 7: Orthophoto mosaic of the FIA1 S-Wall1 (a) and N-Wall (c): the yellow dashed line is the top of the lava flow, the green dashed line is an erosive surface interesting the tops of U2 and the lava flow, the inferred fault planes are shown in red. b) and (d) reconstruction of the stratigraphic succession along the FIA1 S-Wall1 and N-Wall (mirror); the inferred fault planes in red displace the lava flow and U2. Yellow dot is the sample collected for chemical analysis.

315

In FIA1 S-Wall2 (Fig. 8) five fault planes have been identified displacing *sd*, U2 and U3 (Fig. 8). The faults create 'horst' and 'graben' systems, where in the most depressed areas the thickness of U3 increases (Fig. 8b). The eastward dipping F2 fault shows a vertical displacement of 28 cm along U2 and a dip direction of N50°/70°, while the two W-dipping F1 and F3 faults show a maximum vertical displacement of 19 cm along U2. The F2 appears to displace also R1 with an offset of 15 cm. The

320 F4 and F5 faults are uncertain, appearing to create a horst in *sd* without clearly displacing the units but the erosive surface between U2 and U3 is lowered of about 40 cm. As a result, *sd* also appears to have a total displacement of about 40 cm inside the graben formed by F2 and F4. Considering also F5, *sd* appears to have a total throw >1 m, dipping toward the E. The dip directions of the antithetic faults are consistent with the value observed in the 2018 surface ruptures. The dip direction of F2 is a bit different than the values measured along the 2018 coseismic ruptures because the strike-slip component is not

325 detectable.
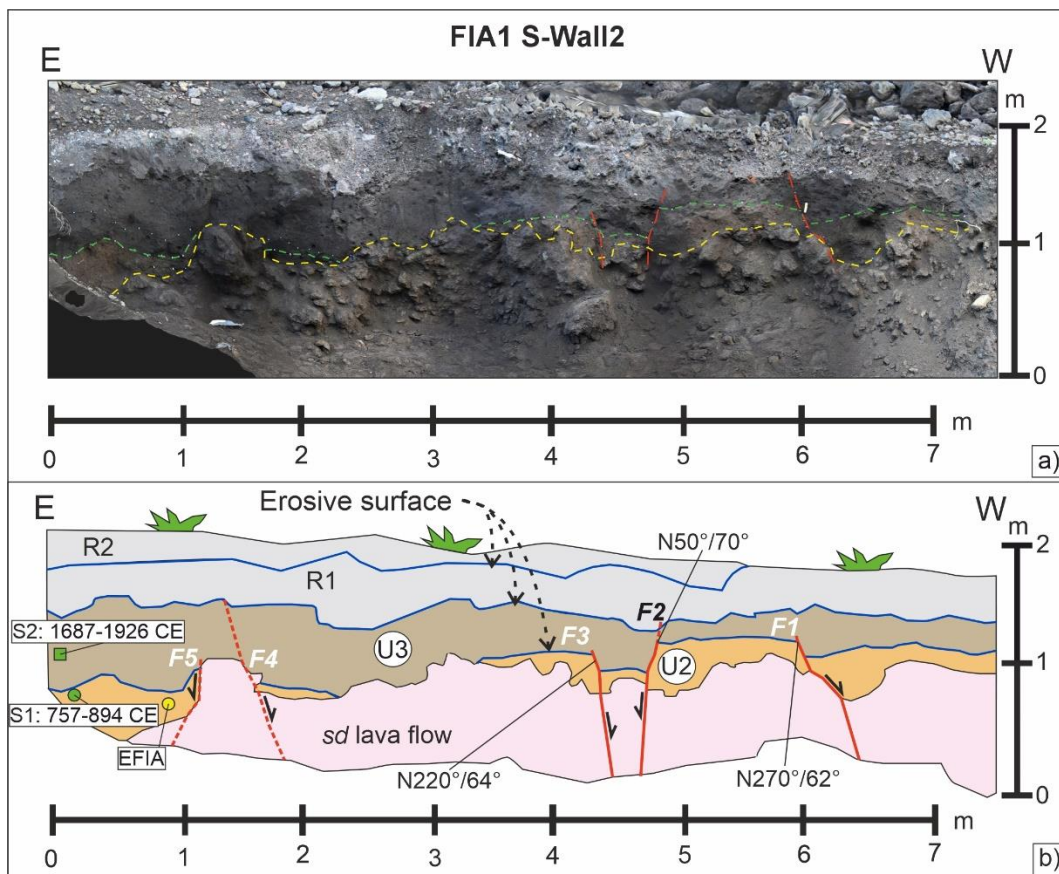
Figure 8: a) Orthophoto mosaic of the FIA1 S-Wall: the yellow dashed line is the top of the lava flow, the green dashed line is top of U2, the fault planes are shown in red. b) reconstruction of the stratigraphic succession along the FIA1 S-Wall; the fault planes in red displace the lava flow, U2, U3 and R; the erosive surfaces are in blue. The green square and dot are dated charcoals (the square corresponds to the opposite wall); yellow dot is the sample collected for chemical analysis.

330

5.3 FIA2 trench

FIA2 N-Wall (Fig. 9) highlights a westward dipping fault (F6) affecting *sd*, U1, U2 and U3 (Fig. 9). U3 shows a vertical displacement of about 15 cm along F6. U2 and U1, on the other hand, show a maximum displacement of 26 cm. On the F6 hanging wall, an open fissure is filled by anthropogenic reworked material in U3 and by the silty sands of U3 in U2 up to the

335 top of U1. The fault F6 is dipping N226°/72° which is consistent with the values measured along the coseismic antithetic 2018 surface ruptures.
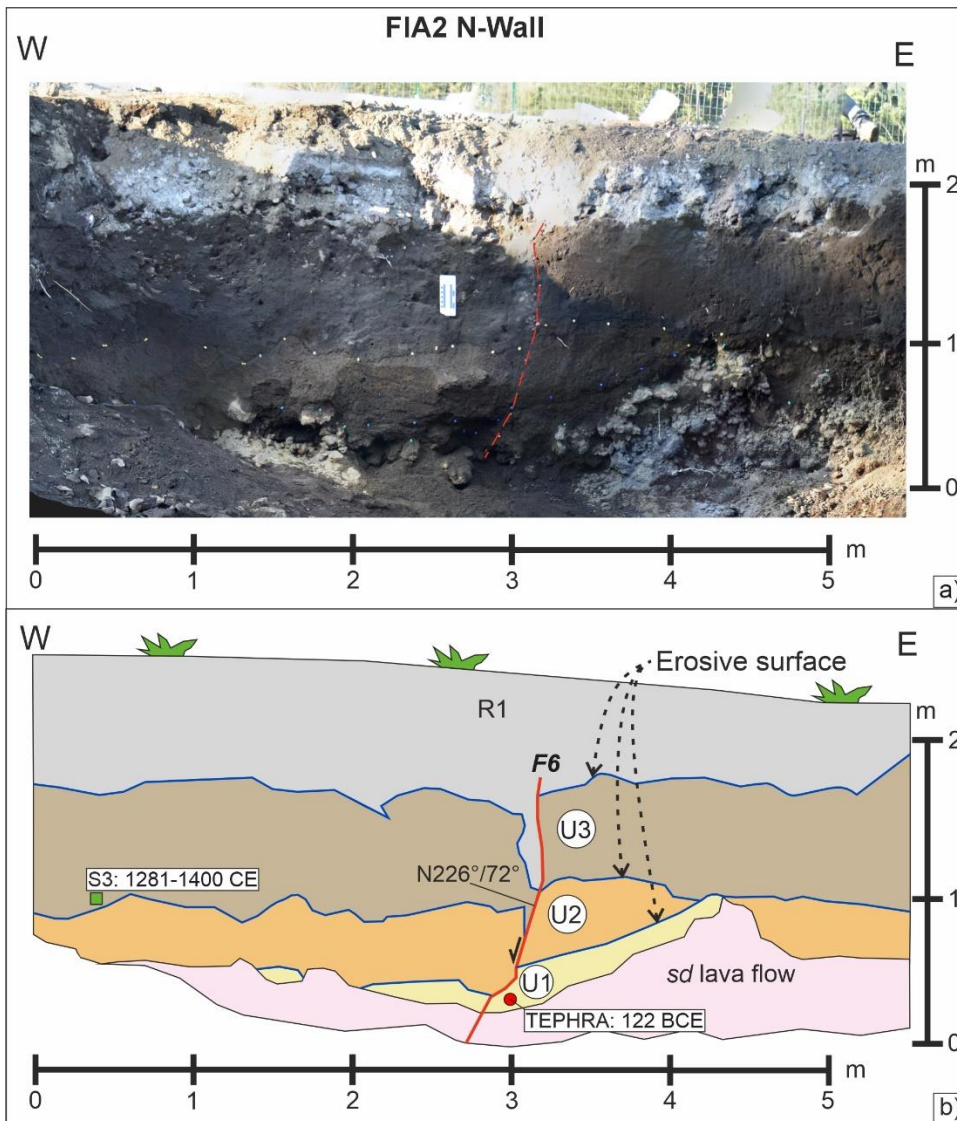
Figure 9: a) Orthophoto mosaic of the FIA2 N-Wall, the coloured pins are between the stratigraphic units and the F6 fault plane (in red); b) reconstruction of the stratigraphic succession along the FIA1 S-Wall, the fault plane in red displaces the lava flow, U1, U2,
340 **U3 and R1. The red dot is the collected tephra sample; the green square corresponds to a dated charcoal along the opposite wall.**

5.4 Fault zone analysis and 2018 ruptures relationships

The analysis of the faults recognized along trenches walls and the ground ruptures highlights a distributed fault deformation zone about 40 m wide which is consistent with 2018 fault rupture width (Tringali et al., 2023a). The faults in the FIA1 S-Wall2 and FIA2, more specifically F2, F4 and F6, correspond with the 2018 coseismic ruptures forming the main fault graben (Figs. 4 and 6a) as well explained in the next chapter. The inferred fault of the FIA1 N-Wall and S-Wall1 is aligned with the 2018 westernmost coseismic ruptures. The *sd* lava flow in the seismic tomography also appears slightly displaced between 4 and 6 m (Fig. 6b) confirming the existence of the inferred fault observed in the FIA1 N-Wall and S-Wall1.

6 Trench restoration and paleoseismic sequence

Previous studies about the Etna eruptions and the dating of charcoal samples allowed to temporal constraint the restoration of the trenches. We conducted this restoration only for the FIA1 S-Wall2 (Fig. 10) and FIA2 N-Wall (Fig. 11), where we found clear evidence of faulting.
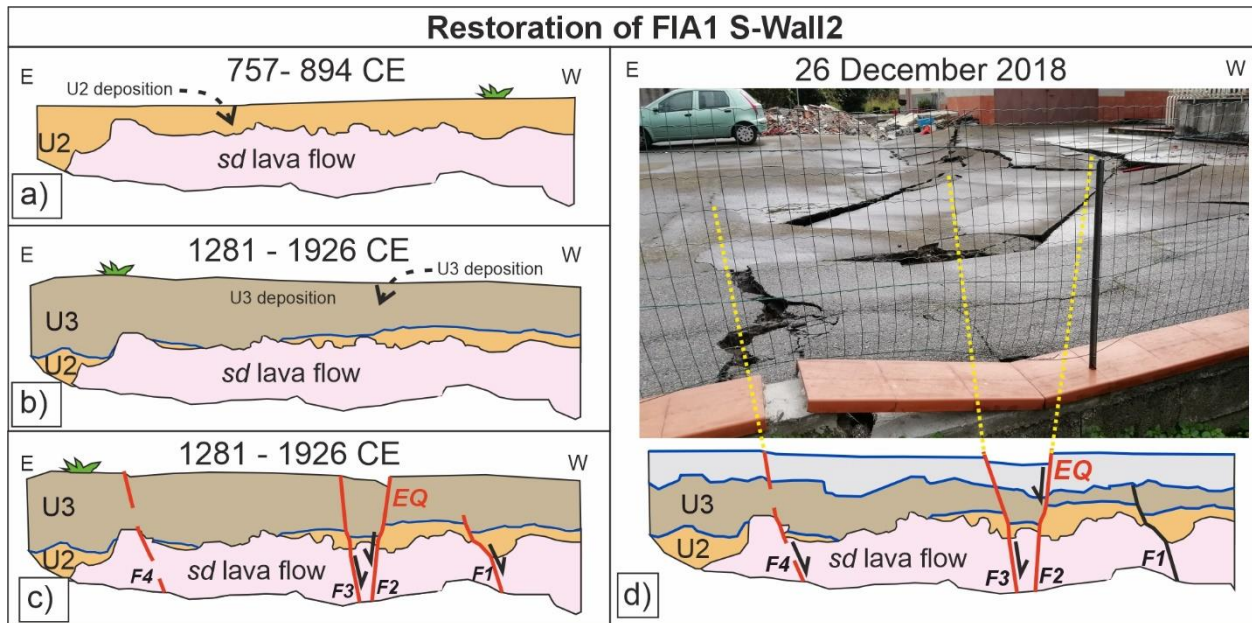
Figure 10: Possible restoration of the FIA1 S-Wall2; a) deposition of the colluvial deposit of U2 during the period 757-894 AD, followed by an erosive event; b) period 1806-1926 AD with the deposition of the colluvial deposit of U3 followed by an earthquake (c) which activated F1, F2, F3 and presumably F4; d) after the reworking of the surface by the human activity and formation of the R1 during the 1970s, a second earthquake in 2018 produced a new surface faulting event along F2 and probably F3 and F4.

According to the dating, it has been possible to identify some seismic events that generally affect all the units. Figure 10 shows the restoration of the FIA1 S-Wall, with two seismic events observed: the first earthquake occurred after or during the

deposition of U3 in the period 1281-1926 CE, and a second one in 2018. In fact, F2 of the FIA1 S-Wall appears to also affect R1, showing evidence of activation during the 2018 event, as this fault corresponds with the 2018 event main surface rupture (Fig. 10d). The supposed F4 corresponds to the antithetic surface rupture of 2018 coseismic graben (Fig. 10d). Probably, the demolition works of the pre-existing building have further reworked R1, thereby obliterating clear evidence of the 2018

365 faulting. The displacements measured along F1, F2, F3 and F4 in FIA1 appear to be consistent with two seismic events in accordance with the throw values observed in the 2018 surface ruptures of the area. Thus, certainly one earthquake occurred along the F1, F2 and F3, but it is very likely that they have undergone two events. If only one earthquake had occurred, this should have been of a higher Mw than the one in 2018 (i.e., Mw>5) given the amount of displacement. However, 5 is the maximum expected Mw estimated for FIA (Azzaro et al., 2017; Azzaro et al., 2022), hence we assume that 2 earthquakes can

370 be observed in FIA1 S-Wall.
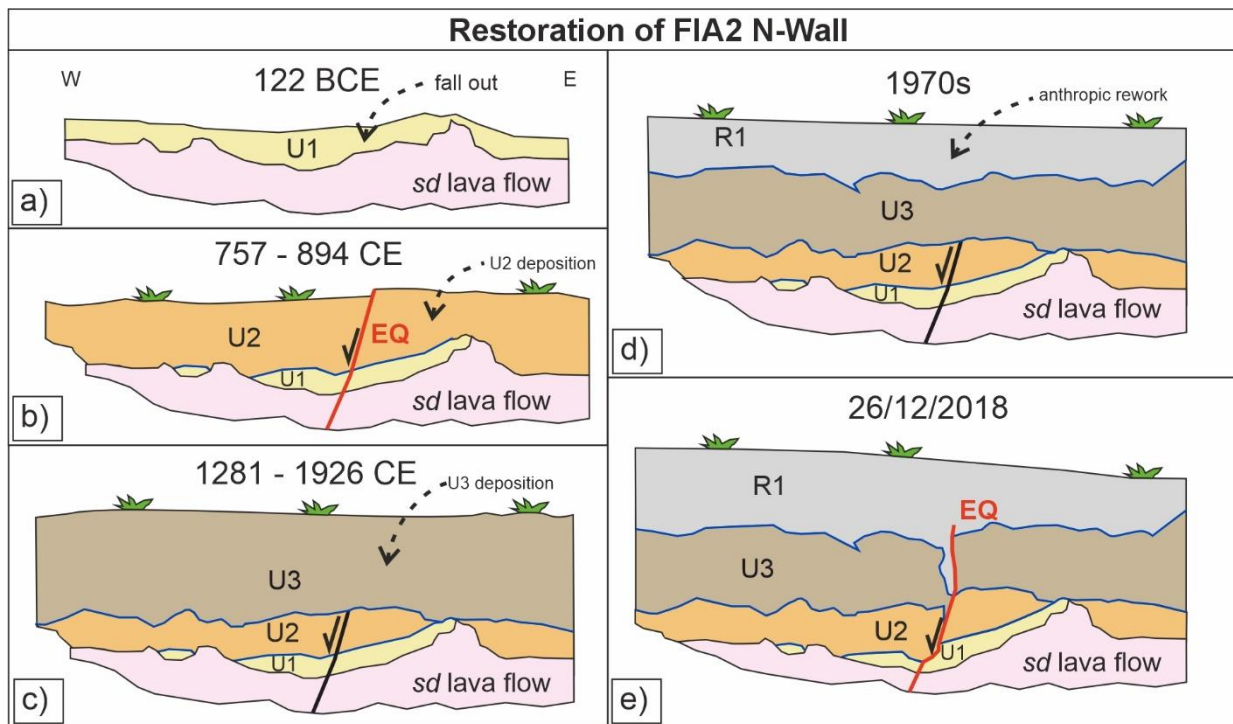
Figure 11: Possible restoration of the FIA2 N-Wall. a) pyroclastic fallout (122 BC Plinian eruption) is deposited on the 150±200 BC lava flow, subsequently eroded; b) an earthquake occurred during the deposition of the colluvial deposit of U2 in the period 757-894

375 **AD; c) after an erosive event on U2, the deposition of the colluvial deposit of U3 occurred in the period 1281-1926 AD; d) reworking of the surface by the human activity and formation of the R1 during the 1970s; e) earthquake in 2018 displacing the lava flow, U1, U2, U3 and R1.**

Regarding the FIA2 N-Wall the F6 displacement of 26 cm measured along U2 and U3 appears to be related to at least two

380 seismic events in accordance with the throw values of the 2018 surface ruptures in the area. Displacement of 15 cm observed

in U3 are consistent with the ones of the 2018 W-dipping surface ruptures occurred exactly in the same location. Moreover, the open fissure along F6 filled by the R1 allows associating it to the 2018 event with a high confidence. The displacement of 26 cm measured in U2 is a minimum, but it can indicate at most least two events when compared with the throw values measured along the 2018 W-dipping surface ruptures. Therefore, also along the FIA2 N-Wall it is possible to infer the occurrence of two earthquakes (Fig. 11).

385 Finally, the combination of the two trenches allow to detect 3 earthquakes (Fig. 12) occurred in: 1) 757-894 CE time interval (Fig. 11b); 2) 1281-1926 CE time interval (Fig. 10c); 3) 26 December 2018 (Figs. 10d and 11e). The first event is a novelty because it is not reported in any seismic catalogue due to the lack of available historical sources so far. Furthermore, this early medieval earthquake might have been triggered by a dyke intrusion related to one of the three eruptions that occurred along 390 the eastern flank in the period 700-850 CE (Branca and Abate, 2017; see Supplementary Table S4). The second event, which preceded the 2018 earthquake, may be associated to the 1894 earthquake, because it is the strongest historical known seismic event with known characteristics. However, there are some uncertainties regarding the precise timing of this event. Certainly, the second event could be associated with another earthquake occurred in the period 1329-1831 CE. Nevertheless, there is no definitive evidence of surface faulting linked to FIA in the historical sources, apart from the 1329 and 1809 CE earthquakes 395 (see Supplementary Table S1). However, the precise location of the ground rupture is not clearly documented.
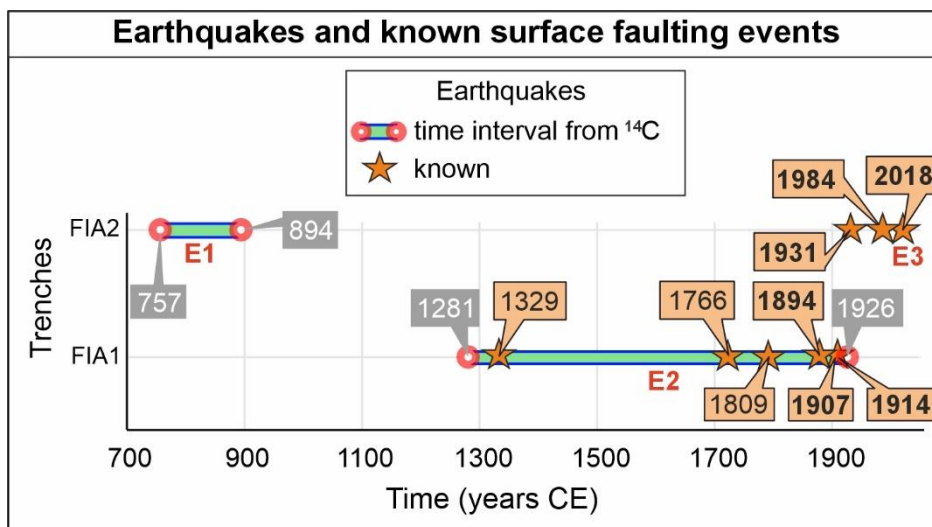
Figure 12: Historical earthquakes, in bold the ones certainly associated with coseismic ruptures along FIA, and time interval of the 3 surface faulting events recognized in the trenches.

400

The highlighted sequence of earthquakes strongly suggests an increase in fault activation over time. In the following chapter, we investigate this hypothesis by examining the temporal variation in Late Pleistocene to historical throw rates along the Fiandaca fault system. We also compare measured Fiandaca fault system throw rates with similar observations on several other capable faults on Mt. Etna eastern flank.

7 Throw rates analysis and flank dynamics

7.1 Throw rates of the Fiandaca fault system

At the Collegio Fiandaca site the lack of information regarding the erosive surfaces and the anthropogenic reworking of a subsurface portion precludes the estimation of total throw-rates based on the observed displacements along the trenches. However, the close interrelationship between FIA, CAT and PLA indicates the presence of a faults system that accommodates the deformation along the lower eastern flank. Thereby, 18 profiles (see traces in Supplementary material; Figs. S1, S2, S3) have been realized along FIA, CAT and PLA, where the Mongibello lava flows and the Valverde formation are displaced to assess the long (~115 ka) and short-term (~1-10 ka) vertical slip rate of the entire fault system. Table A1 (see Appendix A) summarizes minimum fault throw assessed along all the profiles, the corresponding throw rates, and their accuracy. We selected 4 representative profiles (see locations in Fig. 2) showed in Fig. 13a with the reconstruction of the relative geological cross section.
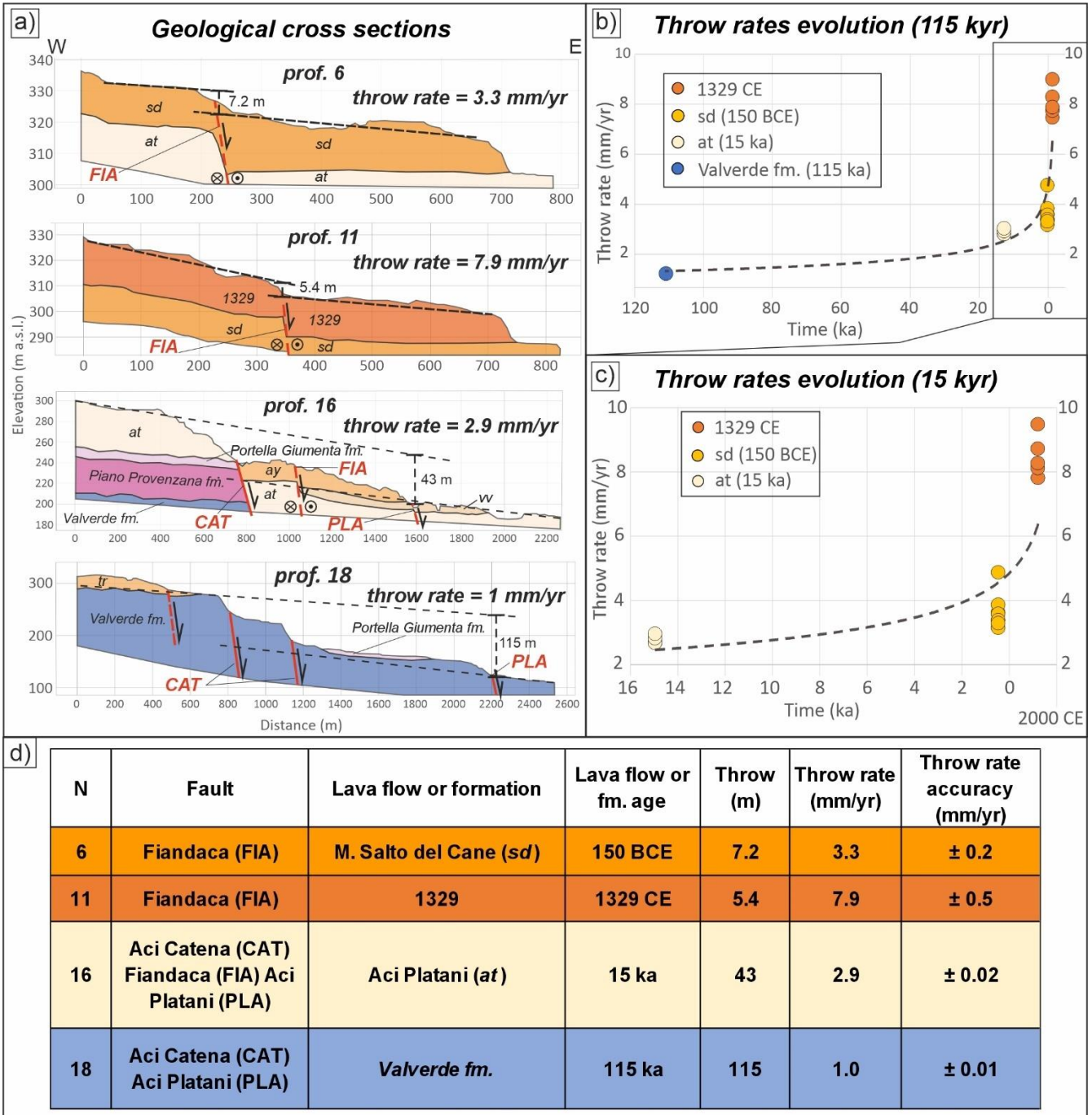
Figure 13: a) selected geological cross sections (vertical exaggeration) along the Fiandaca (6, 11 and 16), Aci Catena and Aci Platani faults (16 and 18); **b)** throw rate evolution for the last 115 kyr and **(c)** 15 kyr; **d)** table showing the characteristics of the topographic profiles.

420

The 115 ka Valverde formation shows a throw of 115 m indicating a minimum throw rate of 1 mm/yr similarly to that reported by Azzaro et al., (2012). The 15 ka *at* shows vertical displacements of ~55 m indicating a minimum throw rate of ~2.9 mm/yr along four profiles. The150 BC *sd* shows an average vertical displacement of ~7.5 m along eight profiles, indicating a throw

425 rate of ~3.3 mm/yr. The 1329 lava flow has vertical displacements of ~6 m from five profiles, indicating a throw rate of 8 mm/yr. The throw rates obtained show an increasing trend through time with a significant growth starting from 1329 CE (Figs. 13b, c and d).

7.2 Throw rates temporal evolution and possible significance

The throw rates analysed are illustrated in Table A2 (see Appendix A) showing literature data (Rasà et al., 1996; Azzaro et al.,

430 1998; Azzaro et al., 2000; Azzaro et al., 2001; Obrizzo et al., 2001; Ferreli et al., 2002; Neri et al., 2007; Bonforte et al., 2011; Azzaro et al., 2012; D'Amato et al., 2017; Tringali, 2023; Tringali et al., 2023b) with the addition of those from this study. These new data include, besides those along the Fiandaca fault system, throw rates obtained from profiles (see location in Supplementary Figs. S2b and S3) along the Trecastagni, San Leonardello and Santa Tecla faults (see Table A1).

The analysis of the throw rates evolution over time (Fig. 14) allows to observe a gradually increase starting at least from the

435 Holocene along the TFS (Fig. 14a) and especially for the PFS (Fig. 14b) and the SFS (Fig. 14c) In particular, during the Late Pleistocene and the Holocene until at least 3.9 ka, throw rates of 0.9-1.4 mm/yr on average occurred along the TFS, PFS and SFS (Fig. 14a, b and c). After 3.9 ka an increase of the throw rates is observed passing from 1.4 to 2.5-3.4 mm/yr on average considering all the faults. Finally, throw rates of ~5-10 mm/yr observed from the Medieval period (Figs. 13c and 14a) suggests a further increase of fault slip events in the last centuries. The highlighted throw rates evolution may be associated with a

440 gradual increase of the flank instability over time. In fact, most of the coseismic and aseismic fault slip events along the eastern flank are triggered by temporary acceleration of the flank sliding. The data corroborate the findings of Acocella and Neri (2005) regarding the PFS. In essence, PFS is comprised of two distinct segments: the western segment (between 1800 and 700 m a.s.l.) and the eastern segment (below 700 m a.s.l.). The eastern part of the fault system is characterised by smaller, separated faults configured in en-échelon pattern, with progressively lower rates of movement towards the Ionian coast. This second part

445 of the fault system resembles a 'neo-fault', in which ground deformation has not yet reached the maturity that characterises the western portion. This suggests a deformation process undergoing recent evolution and expansion, connected with the sliding phenomena that characterise the eastern flank of the volcano. However, it would be erroneous to rule out the possibility that the flank instability process was already acting as previously suggested (Tibaldi and Groppelli, 2002; Groppelli and Norini, 2011), with probable involvement in significant sliding acceleration episodes, albeit less frequent. The observed increase in

450 flank instability can be attributed to the growth of the volcanic edifice over time, which has reached its maximum size in the last 20-30 thousand years.

Even though erosive processes may lead to underestimate the throw rates, some of them gradually increase of 2-4 times, since 15 ka, 3.9 ka and the latest years (e.g., PER, FIU, GRE, 3CA; CAT, PLA, FIA, LEO, TEC; see Fig. 14 and Table A2). The most impressive throw rate increase is along PER (Fig. 14ba), from 2.5 mm/yr in the last 15 kyr to 15-36 mm/yr in the last 3.5

kyr (D'Amico et al., 2017; Ferreli et al., 2002; Obrizzo et al., 2001). GRE also experienced a high increase (Fig. 14c) from 0.3 mm/yr in the last 15 kyr (Azzaro et al., 2012) to 3 mm/yr in the period 1995-2000 (Bonforte et al., 2011), which is consistent with the maximum vertical displacements on manmade structures of 5-10 cm observed since the 1960s (Monaco et al., 2010; Imposa et al., 2015). The increases along PER and GRE are extremely high, one order of magnitude greater, and considering that these two faults play an important role bounding the flank instability (Neri et al., 2004; 2007; Azzaro et al., 2013; Urlaub et al., 2018), it is very likely an increase of the E flank sliding over time.
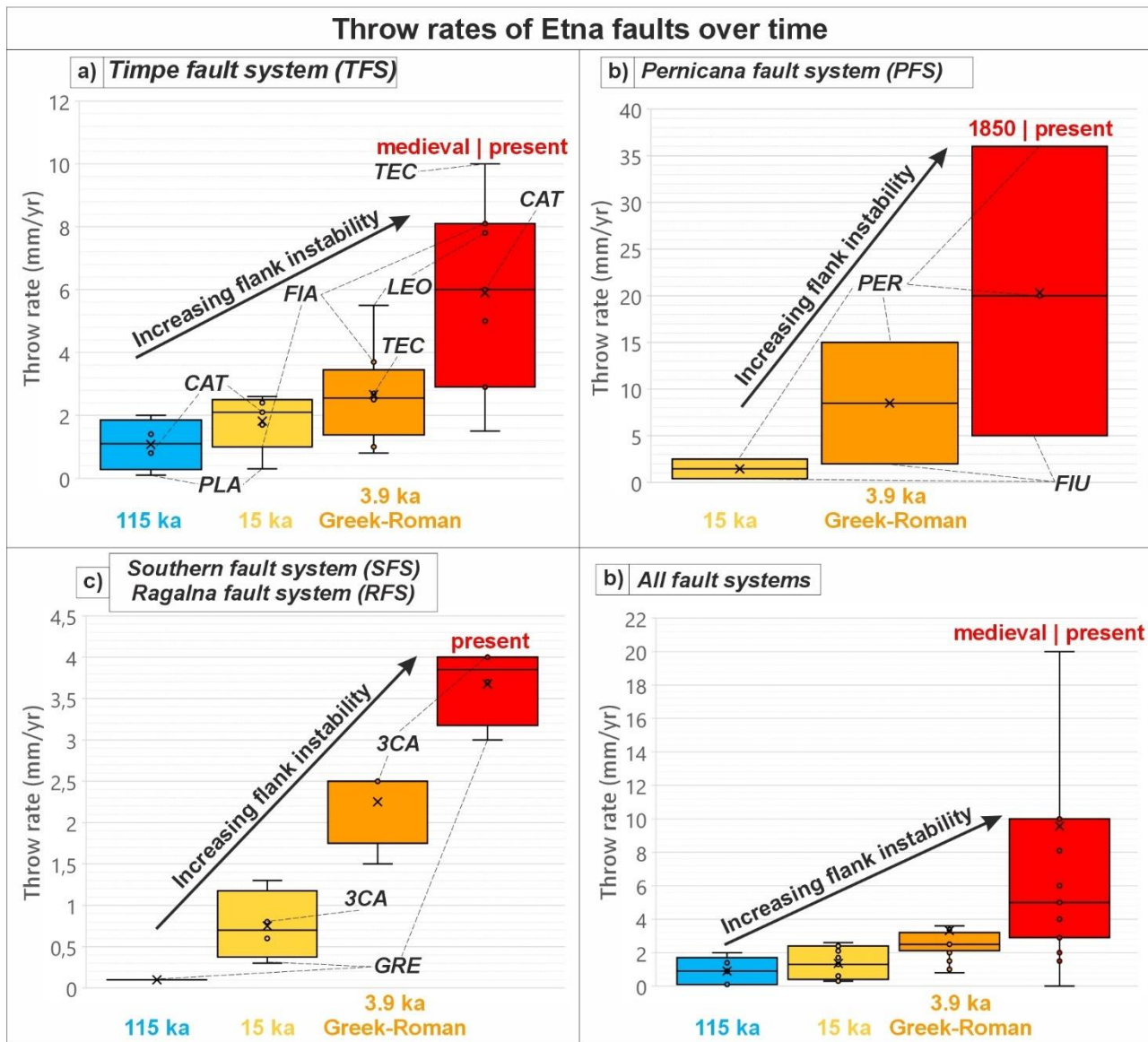
Figure 14: Boxplots of the Etna faults throw rates (see Table A2) highlighting an evolution over time: a) Timpe fault system; b) Pernicana fault system; c) Southern fault system; d) all faults.

465   These findings agree with the recent GNSS data, which shows displacements toward the E higher than 15-20 mm/yr along the TFS with major deformation along the hanging walls (Bonforte and Puglisi, 2006; Carnemolla et al., 2023; Palano et al., 2023). A similar behaviour is observed also along the SFS.

In conclusion, the flank instability was already acting in the Late Pleistocene and in the beginning of the Holocene, albeit with minor sliding velocity. During the Holocene, flank instability gradually increased over time reaching its current sliding rate

470   presumably during the Middle Ages. This led to the superimposition of the current sliding process on the long-term regional tectonic uplift.

7.3 Concurrent factors affecting flank dynamics

The apparent increase in throw rates over time may be related to recent earthquake clusters triggered by dyke intrusions, which have been observed to temporarily accelerate slip along faults (Acocella et al., 2003; Neri et al., 2005; Azzaro et al., 2012).

475   Nonetheless, considering the change in volcanic behaviour over the last centuries, with an increase in flank eruptions, these clusters could become more frequent, thereby impacting flank instability. Thus, when considering long-term eruptive cycles, their impact on volcano flank dynamics may be more significant than those observed during individual eruptive events. For example, the 1669 event, characterized by dry fractures extending approximately 12 km from the base of the central crater along the entire S Rift (Branca et al., 2015), suggests that the magmatic intrusion caused intense deformation on the sliding

480   flank of the volcano. However, considering the entire eruptive cycle of the 17th Century (Behncke and Neri, 2003), it is likely to have affected the flank instability in the long term, influencing subsequent lateral eruptions. For these reasons, an analysis of the spatial and temporal distribution of historical flank eruptions and relative eruptive fissures (see locations in Fig. 1) was carried out revealing a variation that generally affects all the Rifts, except for the S one which seems to maintain roughly a constant activity (Fig. 15). In general, a change is observed from 1000 CE onwards with a significant increase in eruptions

485   along the NE Rift (Figs. 15a and b). More specifically, last centuries flank eruptions, following the 1700, have become more frequent at higher altitude along the NE and S Rifts (Fig. 15c), which border the eastern instability sector. The increase in throw rates along PER may be associated with more frequent dyke intrusions along the NE Rift (D'Amato et al., 2017). Conversely, few eruptions interested the W Rift which was very active during the Greek-Roman period (Fig. 15a) and over the long term (Fig. 15d; Branca and Abate, 2019). This could also be due to the fact that the W Rift may host a greater number

490   of 'eccentric' or 'peripheral' eruptions, i.e. fed by magma conduits other than the central one, which allow magma to rise vertically to the surface rather than laterally, and thus make a minor contribution to the movements of the eastern flank of the volcano (Neri et al., 2011; Acocella et al., 2013). Furthermore, an apparent increase of eruptive fissures is also observed in the ENE flank (Fig. 14b, c and d), aligning with an extension toward the ESE of the eastern flank. This grow may be associated with the increasing of the gravitational sliding that can promote the capture of the uprising magma in the eastern flank along

495   NAC as happened during the 1928 eruption (Tibaldi et al., 2021, 2022). This magma capture supports the hypothesis that NAC represents a deep structure inherited from the sedimentary basement (Azzaro et al., 2012).
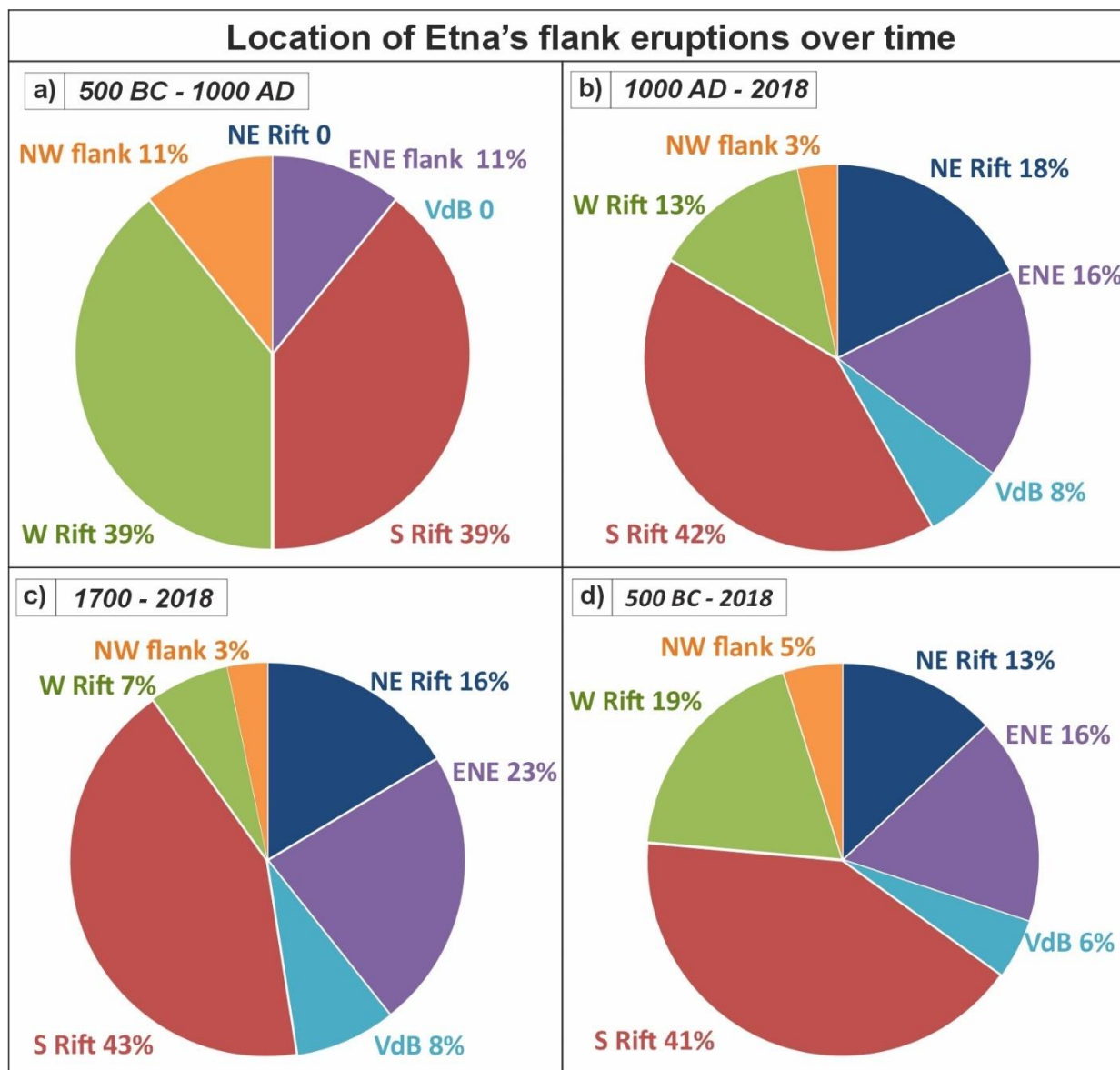
Figure 15: Etna historical eruptive fissures spatial and temporal distribution (see supplementary Tables S4 and S5): a) 500 BC –
1000 AD period; b) 1000 AD – 2018 period; c) 1700 – 2018 period; d) 500 BC – 2018 period. VdB: Valle del Bove eruptions with
uncertain location of the eruptive fissures; ENE: East-Northeast flank strictly related to the NAC fault zone.

The feedback processes occurring between flank instability and lateral eruptions at Mt. Etna (i.e., 1989, 1991-1993, 2001,
2002-2003, 2004-2005 eruptions) have been explored in several works (Acocella et al., 2003; Bonforte and Puglisi, 2003; Neri
et al., 2005; Walter et al., 2005a; Neri and Acocella, 2006; Bonaccorso et al., 2013; Bonforte et al., 2019). Several authors
have described the combination of volcano spreading and flank sliding as controlling the position of future eruptive events
through the creation of shallow fractures and weaknesses that become the paths of rising magma (see McGuire and Pullen,

1989; Acocella and Neri, 2003; Acocella and Tibaldi, 2005; Ruch et al., 2012; Pezzo et al., 2020). Furthermore, analogue structural evolution modelling of La Palma and multidisciplinary studies in Tenerife (Canary Islands) suggests that the position and the direction of the main volcanic rifts are guided by the flank instability (Walter and Troll, 2003; Walter et al., 2005b). Therefore, even considering the importance of the regional tectonics in driving magma from the deep plumbing system, the recent increase of the volcano-tectonic activity with more eruptions in the upper flanks, seismicity and surface faulting events may be explained with an increase of the flank instability.

If the observed trend will persist, it could lead to a further increase in eruptions, seismicity, and surface faulting events with consequences in the associated hazards. Flank instability is a major issue in the coastal and insular volcanoes because it may lead to catastrophic collapses that can also trigger dangerous tsunamis. This is even more important in a volcano like Etna, which is inhabited by around a million people, most of whom are concentrated on its southern and eastern flanks, the most affected by deformation. Although a catastrophic scenario is unlikely, a collapse that may partially involve the inhabited eastern slope cannot be completely ruled out. For these reasons, it will be important to investigate the hypothesis of the increase of the flank instability with i) extensive paleoseismological investigations to better estimate the fault's slip-rates; ii) advanced studies on the spatial and temporal distribution of the flank eruptions; and iii) the improving of the volcano monitoring system, especially along active and capable faults.

8 Conclusions and future perspectives

Recent shallow earthquakes damage and associated flank eruptions on Mt. Etna have allowed the study of the dynamics of the Etna's eastern flank with multidisciplinary approaches. The first paleoseismological evidence along the Fiandaca Fault prompted the identification of three earthquakes occurring:

i.   in the Early Middle Ages (i.e., 757-894 CE);

ii.   in the period spanning the recent centuries (i.e., 1281-1926 CE), may be considered to correspond to the date of 8 August 1894;

iii.   the 26 December 2018.

At present we have no record in any seismic catalogue of the earthquake that occurred in the Early Middle Ages. We may speculate that it was triggered by the dyke intrusion associated with one of the three flank eruptions, reported in Branca and Abate (2019), that took place along the eastern flank during the same period. The 2018 surface faulting correspond to the faults recognized within the trenches and during field survey immediately after the earthquake. This evidence confirms the importance of paleoseismology and exploratory stratigraphic trenches for the seismic risk reduction also in volcanic contexts. In addition, these paleoseismic results suggest an increase of seismicity and fault activation through time.

The analysis of throw rates variations over time obtained along different lava flows along the Fiandaca-Aci Catena-Aci Platani faults scarps, reveals an increase in throw rates from 1.4 mm/yr at the beginning of Holocene to 8 mm/yr starting from the Medieval period onwards. These results corroborate the paleoseismic findings. Furthermore, an increase in throw rates has

540   been observed in numerous other eastern flank faults (TFS, PFS, SFS and RFS in Fig. 14), particularly those situated adjacent
       to regions exhibiting flank sliding such as the Pernicana and San Gregorio faults (PER and GRE in Fig. 14). This behavioural
       pattern suggests an increase in flank instability over time. This is findings are in alignment with recent geodetic data but also
       with the continuous growing of the volcanic edifice which reached its maximum size at the end of the Pleistocene.

       It seems highly probable that increase in flank instability has influenced the eruptive activity of the last few centuries, resulting

545   in the opening of new eruptive fissures at higher altitudes on the eastern flank along the NE and S Rifts, as well as along the
       Ripe della Naca faults. Nevertheless, it cannot be discounted that the acceleration of flank deformations was triggered by an
       increase in the frequency and quantity of magma moving from the deep magma chamber to the surface layers of the crust,
       which could undergo cyclical secular variations. However, as emerged in several studies, feedback processes occur between
       flank instability and lateral eruptions, thus, they concurrently act in the flank dynamics. In any case, these recent changes in

550   the flank dynamics have also led to a decrease in volcanic activity along the W Rift, which was more active during the Greek-
       Roman period.

       The observed increase in flank instability is a significant finding, as it may potentially lead to an increase in the frequency of
       eruptions, major earthquakes and surface faulting events, which in turn may result in significant hazards. Moreover, in the
       worst-case scenario it could lead to collapses that would adversely impact a densely populated area. Hence, further

555   investigations are required regarding the past flank eruptions and slip rates, with a view to better constrain the increasing trend
       of the sliding flank.

       It is evident that a multitude of factors contribute to the overall volcanic activity, including regional tectonic movements, the
       intrusion of dikes, lateral eruptions, the slippage along faults, and the instability of the volcano's flank. Consequently, risk
       assessments and future land use planning must adopt a comprehensive approach that considers the potential for a range of

560   hazards.

565

570

Appendix A: Mt. Etna capable faults throw rates

575 **Table A1: Throws and throw rates obtained by 22 geological profiles along several displaced and dated lava flows.**

N	Fault	Lava flow	Age	Throw (m)	Throw rate (mm/yr)	Throw rate accuracy (mm/yr)
1	Fiandaca (FIA)	M. Salto del Cane (sd)	150 BCE	10.5	4.9	±0.2
2	Fiandaca (FIA)	M. Salto del Cane (sd)	150 BCE	7.5	3.5	±0.2
3	Fiandaca (FIA)	M. Salto del Cane (sd)	150 BCE	6.6	3.1	±0.2
4	Fiandaca (FIA)	M. Salto del Cane (sd)	150 BCE	7.6	3.5	±0.2
5	Fiandaca (FIA)	M. Salto del Cane (sd)	150 BCE	8	3.7	±0.2
6	Fiandaca (FIA)	M. Salto del Cane (sd)	150 BCE	7.5	3.5	±0.2
7	Fiandaca (FIA)	M. Salto del Cane (sd)	150 BCE	8.2	3.8	±0.2
8	Fiandaca (FIA)	M. Salto del Cane (sd)	150 BCE	8.1	3.7	±0.2
9	Fiandaca (FIA)	1329	1329 CE	5.2	7.6	±0.5
10	Fiandaca (FIA)	1329	1329 CE	6.8	10.0	±0.5
11	Fiandaca (FIA)	1329	1329 CE	5.5	8.1	±0.5
12	Fiandaca (FIA)	1329	1329 CE	6.0	8.8	±0.5
13	Fiandaca (FIA)	1329	1329 CE	6.5	9.5	±0.5
14	Aci Catena (CAT) Fiandaca (FIA) Aci Platani (PLA)	Aci Platani (at)	15 ka	44	2.9	±0.02
15	Aci Catena (CAT) Fiandaca (FIA) Aci Platani (PLA)	Aci Platani (at)	15 ka	41	2.7	±0.02
16	Aci Catena (CAT) Fiandaca (FIA) Aci Platani (PLA)	Aci Platani (at)	15 ka	43	2.9	±0.02
17	Aci Catena (CAT) Fiandaca (FIA) Aci Platani (PLA)	Aci Platani (at)	15 ka	45	3	±0.02
18	Aci Catena (CAT) Aci Platani (PLA)	Valverde fm.	115 ka	110.0	1.0	±0.01
19	Trecastagni (3CA)	Vigna Grande (vr)	15 ka	11.8	0.8	±0.02
20	San Leonardello (LEO)	M. Ilice (mi)	1030 CE	7.7	7.8	±0.4
21	San Leonardello (LEO)	M. Gorna (mg)	500 BCE	13.8	5.5	±0.2
22	Santa Tecla (TEC)	Piano d'Api (ay)	3.9 ka	10.2	2.6	±0.1

Table A2: Throw rates of the Etna faults according to long and short-term dating, showing a general increase over time. Method for the throw rate estimation: FO: field observation (geomorphological and geological), PT: paleoseismological trench, GD: geodetic
580   **data. Sources indicated in the column References.**

Fault system	Fault	Throw rates (mm/yr)	Time	Method	References
RFS	Calcerana (CAL)	0.6	15 kyr	FO	Azzaro et al., 2012
		2.5	3.9 kyr	FO	Azzaro et al., 2012
	Masseria Cavaliere (CAV)	1.3	15 kyr	FO	Azzaro et al., 2012
		1.5	3.9 kyr	FO	Azzaro et al., 2012
		3.7	1993-2002 CE	FO	Neri et al., 2007
PFS	Pernicana (PER)	1-2.5	15 kyr	FO	D'Amato et al., 2017
		15	3.5 kyr	FO	D'Amato et al., 2017
		20	>1850 CE	FO; PT	Ferreli et al., 2002
		36	1980-1997 CE	FO	Obrizzo et al., 2001
		12	1997-1999 CE	FO	Azzaro et al., 2001
	Fiumefreddo (FIU)	0.4	15 kyr	FO	Azzaro et al., 2012
		2	3.9 kyr	FO	Azzaro et al., 2012
		5	1971-1997 CE	FO	Azzaro et al., 1998
SFS	Tremestieri (3ME)	2.5	3.9 kyr	FO	Azzaro et al., 2012
		4	1995-2000 CE	GD	Bonforte et al., 2011
	Trecastagni (3CA)	0.8	15 kyr	FO	This study
		2.5	3.9 kyr	FO	Azzaro et al., 2012
		4	1995-2000	GD	Bonforte et al., 2011
	San Gregorio (GRE)	0.1	110 kyr	FO	Azzaro et al., 2012
		0.3	15 kyr	FO	Azzaro et al., 2012
		3	1995-2000 CE	GD	Bonforte et al., 2011
TFS	Aci Catena (CAT)	0.9	115 kyr	FO	This study
		1.4	35 kyr	FO	Azzaro et al., 2012
		2.4	15 kyr	FO	This study
		2.6	3.9 kyr	FO	Azzaro et al., 2012
		2.3-3.6	1970-1995	FO	Rasà et al., 1996
		6	1995-2000	GD	Bonforte et al., 2011
	Aci Platani (PLA)	0.1	110 kyr	FO	Azzaro et al., 2012
		0.4	15 kyr	FO	Azzaro et al., 2012
		2.5	3.9 kyr	FO	This study

Fiandaca (FIA)	1.0	3.9 kyr	FO	Azzaro et al., 2012
	3.7	>150 BCE	FO	This study
	8.1	>1329 CE	FO	This study
Santa Tecla (TEC)	2.8	3.9 kyr	FO	This study
	10	1979-1995	FO	Rasà et al., 1996
Scalo Pennisi (SCA)	0.8-1	>500 BCE	FO	Tringali, 2023
	1.5	2002-2022 CE	FO	Tringali et al., 2023b
Moscarello (MOS)	2	100 kyr	FO	Azzaro et al., 2012
	1.7	7.6 kyr	FO	Azzaro et al., 2012
	1.4-2.7	6.0 kyr	FO; PT	Azzaro et al., 2000
	2.5	3.9 kyr	FO	Azzaro et al., 2012
	3	1995-2000 CE	GD	Bonforte et al., 2011
San Leonardello (LEO)	2.6	7.6 kyr	FO	Azzaro et al., 2012
	5.5	>500 BCE	FO	This study
	7.8	>1000 CE	FO	This study
	5	1980-1995 CE	FO	Rasà et al., 1996
Ripe della Naca (NAC)	0.7	180-15 kyr	FO	Azzaro et al., 2012

Data availability

The data about Fiandaca historic surface faulting events, geological cross sections with associated traces on maps, and eruptive history that support the findings of this study are available in the supplement of this article. Data about historical and instrumental seismicity can be found in the: CFTI5MEd (https://storing.ingv.it/cfti/cfti5/); CMTE
585 (https://www.ct.ingv.it/macro/etna/index.html). Spatial and structural data about the 2018 surface ruptures are available in the zenodo repository (https://zenodo.org/records/8414945).

Supplement

The supplement related to this article is available online.

Author contributions

590 Conceptualization of the study was done by GT. Field work investigations was performed by GT, DB, AMM, FL, AMB, LG, and ST. VA performed the UAV survey and processed the acquired data. RP performed the geophysical survey and processed the seismic refraction data acquired. The data analysis was performed by GT with help from FL and GG. The interpretation of the results was done by GT with help from DB, FL, GG, MN and AMM. The writing of the original draft and preparation of figures was done by GT with help from all co-authors. All authors read, revised and approved the final paper.

Competing interests

The authors declare that they have no conflict of interest.

Acknowledgements

We are grateful to the owners of the Collegio Fiandaca site for allowing us the excavation of the trenches. We are indebted with Mauro Coltelli for visiting the trenching site, analysing the tephra sample and for providing us detailed information about the 122 BCE pyroclastic deposit, but also for the fruitful scientific discussions. This work was part of the Giorgio Tringali PhD project carried out at the University of Insubria (Italy).

Financial support

Research funded by European Union – NextGenerationEU – Mission 4 "Education and Research" – Component 2 "From Research to Business" – Investment 3.1 "Fund for the realization of an integrated system of research and innovation infrastructures" – Project IR0000037 – GeoSciences IR - CUP I53C22000800006

References

Acocella, V., Behncke, B., Neri, M., and D'Amico, S.: Link between major flank slip and 2002–2003 eruption at Mt. Etna (Italy), Geophys. Res. Lett., 30, 2286, https://doi.org/10.1029/2003GL018642, 2003.

Acocella, V., and Neri, M.: What makes flank eruptions? The 2001 Etna eruption and its possible triggering mechanisms. Bulletin of Volcanology, 65, 517-529, https://doi.org/10.1007/s00445-003-0280-3, 2003.

Acocella, V. and Neri, M.: Structural features of an active strike-slip fault on the sliding flank of Mt. Etna (Italy). J. Structural Geology, 27/2, pp. 343-355, https://doi.org/10.1016/j.jsg.2004.07.006, 2005.

Acocella, V., Neri, N., Behncke, B., Bonforte, A., Del Negro, C. and Ganci. G.: Why does a mature volcano need new vents? The case of the New Southeast Crater at Etna, Front. Earth Sci. 4:67, https://doi.org/10.3389/feart.2016.00067, 2016.

Acocella, V., Neri, M. and Norini, G.: An overview of analogue models to understand a complex volcanic instability: application to Etna, Italy, J. of Volcanology and Geothermal Research, 251, 98–111,https://doi.org/10.1016/j.jvolgeores.2012.06.003, 2013.

Acocella, V., and Tibaldi, A.: Dike propagation driven by volcano collapse: a general model tested at Stromboli, Italy, Geophysical Research Letters, 32(8), https://doi.org/10.1029/2004GL022248, 2005.

Azzaro, R.: Earthquake surface faulting at Mount Etna volcano (Sicily) and implications for active tectonics, J. of Geodynamics 28, 193–213, https://doi.org/10.1016/S0264-3707(98)00037-4, 1999.

Azzaro, R., Barberi, G., D'Amico, S., Pace, B., Peruzza, L., and Tuvè, T.: When probabilistic seismic hazard climbs volcanoes: the Mt. Etna case, Italy – Part 1: Model components for sources parameterization, Nat. Hazards Earth Syst. Sci., 17, 1981–1998, https://doi.org/10.5194/nhess-17-1981-2017, 2017.

Azzaro, R., Bella, D., Ferreli, L., Michetti, A. M., Santagati, F., Serva, L., and Vittori, E.: First study of fault trench stratigraphy at Mt. Etna volcano, Southern Italy: understanding Holocene surface faulting along the Moscarello fault, J. of Geodynamics, 29(3-5), 187-210, https://doi.org/10.1016/S0264-3707(99)00055-1, 2000.

Azzaro, R., Branca, S., Gwinner, K., and Coltelli, M.: The volcano-tectonic map of Etna volcano, 1: 100.000 scale: an integrated approach based on a morphotectonic analysis from high-resolution DEM constrained by geologic, active faulting and seismotectonic data, Italian Journal of Geosciences, 131(1), 153-170, https://doi.org/10.3301/IJG.2011.29, 2012.

Azzaro, R., Bonforte, A., Branca, S. and Guglielmino, F.: Geometry and kinematics of the fault systems controlling the unstable flank of Etna volcano (Sicily), J. of Volcanology and Geothermal Research 251, 5–15, https://doi.org/10.1016/j.jvolgeores.2012.10.001, 2013.

Azzaro, R., Ferreli, L., Michetti, A.L., Serva, L. and Vittori, E.: Environmental hazard of capable faults: the case of the Pernicana fault (Mt. Etna, Sicily), Nat. Haz., 17 (2), 147-162, https://doi.org/10.1023/A:1008034422086, 1998.

Azzaro, R., and Castelli, V.: Materiali per un catalogo di terremoti etnei dal 1600 al 1831. Quaderni di Geofisica, 123, 284 pp., https://doi.org/10.13127/qdg/123, 2015.

Azzaro, R., Mattia, M., and Puglisi, G.: Fault creep and kinematics of the eastern segment of the Pernicana Fault (Mt. Etna, Italy) derived from geodetic observations and their tectonic significance, Tectonophysics, 333(3-4), 401-415, https://doi.org/10.1016/S0040-1951(01)00021-X, 2001.

Azzaro, R., Pucci, S., Villani, F., Civico, R., Branca, S., Cantarero, M., et al.: Surface faulting of the 26 December 2018, Mw5 earthquake at Mt. Etna volcano (Italy): Geological source model and implications for the seismic potential of the Fiandaca fault. Tectonics, 41, e2021TC007182. https://doi.org/10.1029/2021TC007182, 2022.

Barreca, G., Bonforte, A., and Neri, M.: A pilot GIS database of active faults of Mt. Etna (Sicily): A tool for integrated hazard evaluation, J. of Volcanology and Geothermal Research, 251, 170-186, https://doi.org/10.1016/j.jvolgeores.2012.08.013, 2013.

Behncke, B., and Neri, M.: Cycles and trends in the recent eruptive behaviour of Mount Etna (Italy). Canadian Journal of Earth Sciences, 40(10), 1405-1411, https://doi.org/10.1139/E03-052, 2003.

Behncke, B., Neri, M., and Nagay, A.: Lava flow hazard at Mount Etna (Italy): new data from a GIS-based study, Special Papers-Geological Society Of America, 396, 189, https://doi.org/10.1130/0-8137-2396-5.189, 2005.

Bevilacqua, A., Azzaro, R., Branca, S., D'Amico, S., Flandoli, F., and Neri, A.: Quantifying the statistical relationships between flank eruptions and major earthquakes at Mt. Etna volcano (Italy), J. of Geophysical Research: Solid Earth, 127(8), e2022JB024145, https://doi.org/10.1029/2022JB024145, 2022.

Bonaccorso, A., Currenti, G., and Del Negro, C.: Interaction of volcano-tectonic fault with magma storage, intrusion and flank
655 instability: A thirty years study at Mt. Etna volcano, J.of Volcanology and Geothermal Research, 251, 127-136,
https://doi.org/10.1016/j.jvolgeores.2012.06.002, 2013.

Bonforte, A., Federico, C., Giammanco, S., Guglielmino, F., Liuzzo, M. and Neri M.: Soil gases and SAR data reveal hidden
faults on the sliding flank of Mt. Etna (Italy), J. of Volcanology and Geothermal Research, 251, 27–40,
https://doi.org/10.1016/j.jvolgeores.2012.08.010, 2013.

660 Bonforte, A., Guglielmino, F., Coltelli, M., Ferretti, A. and Puglisi, G.: Structural assessment of Mount Etna volcano from
Permanent Scatterers analysis, Geochemistry, Geophysics, Geosystems 12, https://doi.org/10.1029/2010GC003213, 2011.

Bonforte, A., Guglielmino, F. and Puglisi, G.: Large dyke intrusion and small eruption: The December 24, 2018 Mt. Etna
eruption imaged by Sentinel-1 data, Terra Nova 31, 405–412, https://doi.org/10.1111/ter.12403, 2019.

Bonforte, A., and Puglisi, G.: Magma uprising and flank dynamics on Mount Etna volcano, studied using GPS data (1994–
665 1995), J. of Geophysical Research: Solid Earth, 108(B3), https://doi.org/10.1029/2002JB001845, 2003.

Bonforte, A., and Puglisi, G.: Dynamics of the eastern flank of Mt. Etna volcano (Italy) investigated by a dense GPS network,
J. of Volcanology and Geothermal Research, 153(3-4), 357-369, https://doi.org/10.1016/j.jvolgeores.2005.12.005, 2006.

Borgia, A., Ferrari, L. and Pasquarè, G.: Importance of gravitational spreading in the tectonic and volcanic evolution of Mount
Etna, Nature 357, 231–235, https://doi.org/10.1038/357231a0,1992.

670 Branca, S., and Abate, T.: Current knowledge of Etna's flank eruptions (Italy) occurring over the past 2500 years. From the
iconographies of the XVII century to modern geological cartography, J. of Volcanology and Geothermal Research, 385, 159-
178, https://doi.org/10.1016/j.jvolgeores.2017.11.004, 2019.

Branca, S., Azzaro, R., De Beni, E., Chester, D., and Duncan, A.: Impacts of the 1669 eruption and the 1693 earthquakes on
the Etna Region (Eastern Sicily, Italy): An example of recovery and response of a small area to extreme events, J. of
675 Volcanology and Geothermal Research, 303, 25-40, https://doi.org/10.1016/j.jvolgeores.2015.07.020, 2015.

Branca, S. and Del Carlo, P.: Types of eruptions of Etna volcano AD 1670–2003: implications for short-term eruptive
behaviour, Bulletin of Volcanology, 67, 732-742, https://doi.org/10.1007/s00445-005-0412-z, 2005.

Branca, S. and Ferrara, V.: The morphostructural setting of Mount Etna sedimentary basement (Italy): Implications for the
geometry and volume of the volcano and its flank instability, Tectonophysics 586, 46–64m,
680 https://doi.org/10.1016/j.tecto.2012.11.011, 2013.

Branca, S., Coltelli, M., and Groppelli, G.: Geological evolution of a complex basaltic stratovolcano: Mount Etna, Italy, Ital.
J. Geosci, 130(3), 306-317, https://doi.org/10.3301/IJG.2011.13, 2011a.

Branca, S., Coltelli, M., Groppelli, G., and Lentini, F.: Geological map of Etna volcano, 1: 50,000 scale, Ital. J.of Geosci.,
130(3), 265-291, https://doi.org/10.3301/IJG.2011.15, 2011b.

685 Branca, S., De Guidi, G., Lanzafame, G., and Monaco, C.: Holocene vertical deformation along the coastal sector of Mt. Etna
volcano (eastern Sicily, Italy): implications on the time–space constrains of the volcano lateral sliding. J. of Geodynamics, 82,
194-203, https://doi.org/10.1016/j.jog.2014.07.006, 2014.

Calvari, S. and Groppelli, G.: Relevance of the Chiancone volcaniclastic deposit in the recent history of Etna Volcano (Italy), J. of Volcanology and Geothermal Research, 72(3-4), 239-258, https://doi.org/10.1016/0377-0273(96)00012-1, 1996.

690 Calvari, S., Tanner, L. H., and Groppelli, G.: Debris-avalanche deposits of the Milo Lahar sequence and the opening of the Valle del Bove on Etna volcano (Italy), J. of Volcanology and Geothermal Research, 87(1-4), 193-209, https://doi.org/10.1016/S0377-0273(98)00089-4, 1998.

Calvari, S., Tanner, L. H., Groppelli, G., and Norini, G.: Valle del Bove, eastern flank of Etna volcano: a comprehensive model for the opening of the depression and implications for future hazards, In Etna Volcano Laboratory (eds A. Bonaccorso, S.

695 Calvari, M. Coltelli, C. Del Negro and S. Falsaperla), American Geophysical Union, https://doi.org/10.1029/143GM05, 2004.

Carnemolla, F., De Guidi, G., Bonforte, A., Brighenti, F., and Briole, P.: The ground deformation of the south-eastern flank of Mount Etna monitored by GNSS and SAR interferometry from 2016 to 2019, Geophysical Journal International, 234(1), 664-682, https://doi.org/10.1093/gji/ggad088, 2023.

Carveni, P. and Bella, D.: Aspetti geomorfologici legati ad attività sismica su vulcani attivi: il basso versante orientale dell'Etna
700 come modello di studio, Boll. Acc. Gioenia Sc. Nat 27, 253–285, 1994.

Carveni, P., Bella, D., Benfatto, S., Maniscalco, R., Puntillo, M. S., and Sturiale, G.: Sollevamenti a grande scala e conseguenti fenomeni gravitativi: l'esempio del versante orientale dell'Etna (Sicilia), Alpine and Mediterranean Quaternary, 18(2), 157-171, 2005.Chiocci, F. L., Coltelli, M., Bosman, A., and Cavallaro, D.: Continental margin large-scale instability controlling the flank sliding of Etna volcano, Earth and Planetary Science Letters 305, 57–64, https://doi.org/10.1016/j.epsl.2011.02.040,
705 2011.

Civico, R., Pucci, S., Nappi, R., Azzaro, R., Villani, F., Pantosti, D.,et al.: Surface ruptures following the 26 December 2018, Mw 4.9, Mt. Etna earthquake, Sicily (Italy): EMERGEO Working Group (Etna 2018), J. of Maps, 15(2), 831-837, https://doi.org/10.1080/17445647.2019.1683476, 2019.

Coltelli, M., Del Carlo, P., and Vezzoli, L.: Discovery of a Plinian basaltic eruption of Roman age at Etna volcano, Italy,
710 Geology, 26(12), 1095-1098, https://doi.org/10.1130/0091-7613(1998)026%3C1095:DOAPBE%3E2.3.CO;2, 1998.

D'Amato, D., Pace, B., Di Nicola, L., Stuart, F. M., Visini, F., Azzaro, R., Branca, S., and Barfod, D. N.: Holocene slip rate variability along the Pernicana fault system (Mt. Etna, Italy): Evidence from offset lava flows, GSA Bulletin, 129(3-4), 304-317, https://doi.org/10.1130/B31510.1, 2017.

De Novellis, V., Atzori, S., De Luca, C., Manzo, M., Valerio, E., Bonano, M., et al.: DInSAR analysis and analytical modeling
715 of Mount Etna displacements: The December 2018volcano-tectonic crisis, Geophysical Research Letters,46. https://doi.org/10.1029/2019GL082467, 2019.

Del Carlo, P., Vezzoli, L., and Coltelli, M.: Last 100 ka tephrostratigraphic record of Mount Etna, In Mt. Etna: Volcano Laboratory (eds A. Bonaccorso, S. Calvari, M. Coltelli, C. Del Negro and S. Falsaperla), Geophysical Monograph Series, 143, 77-89, https://doi.org/10.1029/143GM06, 2004.

720 Doglioni, C., Innocenti, F. and Mariotti, G.: Why Mt Etna? Terra Nova 13, 25–31, https://doi.org/10.1046/j.1365-3121.2001.00301.x, 2001.

Firetto Carlino, M., Cavallaro, D., Coltelli, M., Cocchi, L., Zgur, F., and Patanè, D.: Time and space scattered volcanism of Mt. Etna driven by strike-slip tectonics, Scientific Reports, 9(1), 12125, https://doi.org/10.1038/s41598-019-48550-1, 2019.

Ferreli, L., Michetti, A., Serva, L., and Vittori, E.: Stratigraphic evidence of coseismic faulting and aseismic fault creep from exploratory trenches at Mt. Etna volcano (Sicily, Italy), Geological Society Of America Bulletin, 359, 49-62, https://doi.org/10.1130/0-8137-2359-0.49, 2002.

Gresta, S., Bella, D., Musumeci, C., and Carveni, P.: Some efforts on active faulting processes (earthquakes and aseismic creep) acting on the eastern flank of Mt. Etna (Sicily), Acta Vulcanologica, 9, 101-108, 1997.

Groppelli, G. and Norini, G.: Geology and tectonics of the southwestern boundary of the unstable sector of Mt. Etna (Italy), J. of Volcanology and Geothermal Research 208, 66–75, https://doi.org/10.1016/j.jvolgeores.2011.08.006, 2011.

Gross, F., Krastel, S., Geersen, J., Behrmann, J. H., Ridente, D., Chiocci, F. L., Bialas, J., Papenber, C., Cukur, D., Urlaub, M., and Micallef, A.: The limits of seaward spreading and slope instability at the continental margin offshore Mt Etna, imaged by high-resolution 2D seismic data, Tectonophysics, 667, 63-76, https://doi.org/10.1016/j.tecto.2015.11.011, 2016.

Guest, J. E., Chester, D. K., and Duncan, A. M.: The Valle del Bove, Mount Etna: its origin and relation to the stratigraphy and structure of the volcano, J. of Volcanology and Geothermal Research, 21(1-2), 1-23, https://doi.org/10.1016/0377-0273(84)90013-1, 1984.Guidoboni E., Ferrari G., Tarabusi G., Sgattoni G., Comastri A., Mariotti D., Ciuccarelli C., Bianchi M.G., Valensise G.: CFTI5Med, the new release of the catalogue of strong earthquakes in Italy and in the Mediterranean area, Scientific Data 6, Article number: 80, https://doi.org/10.1038/s41597-019-0091-9, 2019.

Imposa, S., De Guidi, G., Grassi, S., Scudero, S., Barreca, G., Patti, G., and Boso, D.: Applying geophysical techniques to investigate a segment of a creeping fault in the urban area of San Gregorio di Catania, southern flank of Mt. Etna (Sicily—Italy), J. of Applied Geophysics, 123, 153-163, https://doi.org/10.1016/j.jappgeo.2015.10.008, 2015.

ITHACA Working Group: ITHACA (ITaly HAzard from CApable faulting), A database of active capable faults of the Italian territory, Version December 2019; ISPRA Geological Survey of Italy. Web Portal http://sgi2.isprambiente.it/ithacaweb/Mappatura.aspx, 2019.

Lanzafame, G., and Bousquet, J. C.: The Maltese escarpment and its extension from Mt. Etna to Aeolian Islands (Sicily): importance and evolution of a lithosphere discontinuity, Acta Vulcanologica, 9, 113-120, 1997.

Lanzafame, G., Neri, M. and Rust, D.: A preliminary structural evaluation of recent tectonic activity on the eastern flank of Mount Etna, Sicily, West London Papers in Environmental Studies, 3, 73-90, 1996.

Lo Giudice, E., and Rasà, R.: Very shallow earthquakes and brittle deformation in active volcanic areas: The Eatnean region as an example, Tectonophysics, 202(2-4), 257-268, https://doi.org/10.1016/0040-1951(92)90111-I, 1992.

Malaguti, A. B., Branca, S., Speranza, F., Coltelli, M., Del Carlo, P., and Renzulli, A.: Age of the Valle del Bove formation and chronology of the post-collapse flank eruptions, Etna volcano (Italy), J. of Volcanology and Geothermal Research, 434, 107752, https://doi.org/10.1016/j.jvolgeores.2023.107752, 2023.

Mattia, M., Bruno, V., Caltabiano, T., Cannata, A., Cannavo, F., D'Alessandro, W., Di Grazia, G., Federico, C., Giammanco, S., La Spina, A., Liuzzo, M., Longo, M., Monaco, C., Patanè, D., and Salerno, G.: A comprehensive interpretative model of

slow slip events on Mt. Etna's eastern flank, Geochemistry, Geophysics, Geosystems, 16(3), 635-658, https://doi.org/10.1002/2014GC005585, 2015.

Mattia, M., Bruno, V., Montgomery-Brown, E., Patanè, D., Barberi, G., and Coltelli, M.: Combined seismic and geodetic analysis before, during and after the 2018 Mount Etna eruption, Geochemistry, Geophysics, Geosystems, 21, e2020GC009218.

760   https://doi.org/10.1029/2020GC009218, 2020.

McCalpin, J. P.: Paleoseismology, International Geophysics, 95, ISBN: 9780080919980, 615 pp., 2009.

McCalpin, J., Ferrario, F., Figueiredo, P., Livio, F., Grützner, C., Pisarska-Jamroży, M., Quigley, M., Reicherter, K., Rockwell, T., Štěpančíková, P., and Tábořík, P.: New developments in onshore paleoseismic methods, and their impact on Quaternary tectonic studies, Quaternary International, 664, 59-76, https://doi.org/10.1016/j.quaint.2023.03.008, 2023.

765   McGuire, W. J., Pullen, A. D.: Location and orientation of eruptive fissures and feeder-dykes at Mount Etna; influence of gravitational and regional tectonic stress regimes, J. of Volcanology and Geothermal Research, 38(3-4), 0–344, https://doi.org/10.1016/0377-0273(89)90046-2, 1989.

Monaco, C., Tapponnier, P., Tortorici, L., and Gillot, P. Y.: Late Quaternary slip rates on the Acireale-Piedimonte normal faults and tectonic origin of Mt. Etna (Sicily). Earth and Planetary Science Letters, 147(1-4), 125-139,

770   https://doi.org/10.1016/S0012-821X(97)00005-8, 1997.

Monaco, C., Barreca, G., Bella, D., Brighenti, F., Bruno, V., Carnemolla, F., De Guidi, G., Mattia, M., Menichetti, M., Roccheggiani, M., and Scarfì, L: The seismogenic source of the 2018 December 26th earthquake (Mt. Etna, Italy): A shear zone in the unstable eastern flank of the volcano. J. of Geodynamics, 143, 101807, https://doi.org/10.1016/j.jog.2020.101807, 2021.

775   Monaco, C., De Guidi, G., and Ferlito, C.: The morphotectonic map of Mt. Etna, Italian J. of Geosciences, 129(3), 408-428, https://doi.org/10.3301/IJG.2010.11, 2010.

Murray, J. B., and de Vries, B. V. W.: Basement sliding and the formation of fault systems on Mt. Etna volcano, J. of Volcanology and Geothermal Research, 428, 107573, https://doi.org/10.1016/j.jvolgeores.2022.107573, 2022.

Neri, M. and Acocella, V.: The 2004-05 Etna eruption: implications for flank deformation and structural behaviour of the

780   volcano, Journal of Volcanology and Geothermal Research, 158, 195-206, https://doi.org/10.1016/j.jvolgeores.2006.04.022, 2006.

Neri, M., Acocella, V., and Behncke, B.: The role of the Pernicana Fault System in the spreading of Mt. Etna (Italy) during the 2002–2003 eruption, Bulletin of Volcanology, 66, 417-430, https://doi.org/10.1007/s00445-003-0322-x, 2004.

Neri, M., Acocella, V., Behncke, B., Giammanco, S., Mazzarini, F., and Rust, D.: Structural analysis of the eruptive fissures

785   at Mount Etna (Italy), Annals of Geophysics, 54, 5, 464-479, https://doi.org/10.4401/ag-5332, 2011.

Neri, M., Acocella, V., Behncke, B., Maiolino, V., Ursino, A., and Velardita, R.: Contrasting triggering mechanisms of the 2001 and 2002–2003 eruptions of Mount Etna (Italy), J. of Volcanology and Geothermal Research, 144(1-4), 235-255, https://doi.org/10.1016/j.jvolgeores.2004.11.025, 2005.

Neri M., Casu, F., Acocella, V., Solaro, G., Pepe, S., Berardino, P., Sansosti, E., Caltabiano, T., Lundgren, P. and Lanari R.:
790   Deformation and eruptions at Mt. Etna (Italy): a lesson from 15 years of observations, Geophysical Research Letters, 36,
L02309, https://doi.org/10.1029/2008GL036151, 2009.

Neri, M., Garduño, V.H., Pasquarè, G. and Rasà, R. Studio strutturale e modello cinematico della Valle del Bove e del settore
nord-orientale etneo, Acta Vulcanol., 1, 17-24, 1991.

Neri, M., Guglielmino, F. and Rust, D.: Flank instability on Mount Etna: Radon, radar interferometry, and geodetic data from
795   the southwestern boundary of the unstable sector, J. of Geophysical Research, Solid Earth, 112,
https://doi.org/10.1029/2006JB004756, 2007.

Neri, M., Rivalta, E., Maccaferri, F., Acocella, V. and Cirrincione, R.: Etnean and Hyblean volcanism shifted away from the
Malta Escarpment by crustal stresses, Earth and Planetary Science Letters 486, 15–22,
https://doi.org/10.1016/j.epsl.2018.01.006, 2018.Obrizzo, F., Pingue, F., Troise, C., and De Natale, G.: Coseismic
800   displacements and creeping along the Pernicana fault (Etna, Italy) in the last 17 years: a detailed study of a tectonic structure
on a volcano, J. of Volcanology and Geothermal Research, 109(1-3), 109-131, https://doi.org/10.1016/S0377-0273(00)00307-
3, 2001.

Palano, M., Sparacino, F., Gambino, P., D'Agostino, N., Calcaterra, S.: Slow slip events and flank instability at Mt. Etna
volcano (Italy), Tectonophysics, 836, 229414, https://doi.org/10.1016/j.tecto.2022.229414, 2022.

805   Palano, M., Calcaterra, S., Gambino, P., Porfidia, B., and Sparacino, F.: GNSS-based long-term deformation at Mount Etna
volcano (Italy). Results in Geophysical Sciences, 14, 100056, https://doi.org/10.1016/j.ringps.2023.100056, 2023.

Pezzo, G., Palano, M., Tolomei, C., De Gori, P., Calcaterra, S., Gambino, P., and Chiarabba, C.: Flank sliding: A valve and a
sentinel for paroxysmal eruptions and magma ascent at Mount Etna, Italy. Geology, 48(11), 1077-1082,
https://doi.org/10.1130/G47656.1, 2020.

810   Rasà, R., Azzaro, R. and Leonardi, O.: Aseismic creep on faults and flank instability at Mount Etna volcano, Sicily, Geological
Society, London, Special Publications 110, 179–192, https://doi.org/10.1144/GSL.SP.1996.110.01.14, 1996.

Ruch, J., Pepe S., Casu F., Acocella V., Neri M., Solaro G. and Sansosti E.: How do volcanic rift zones relate to flank
instability? Evidence from collapsing rifts at Etna, Geophysical Research Letters 39, L20311,
https://doi.org/10.1029/2012GL053683, 2012.

815   Rust, D., and Neri, M.: The boundaries of large-scale collapse on the flanks of Mount Etna, Sicily, Geological Society, London,
Special Publications, 110(1), 193-208, https://doi.org/10.1144/GSL.SP.1996.110.01.15, 1996.

Siniscalchi, A., Tripaldi,S., Neri, M., Balasco, M., Romano, G., Ruch, J. and Schiavone D.: Flank instability structure of Mt
Etna inferred by a magnetotelluric survey, J. Geophys. Res., 117, B03216, https://doi.org/10.1029/2011JB008657, 2012.

Solaro, G., Acocella, V., Pepe, S., Ruch, J., Neri, M., and Sansosti, E. (2010). Anatomy of an unstable volcano from InSAR:
820   Multiple processes affecting flank instability at Mt. Etna, 1994–2008, J. of Geophysical Research: Solid Earth, 115(B10),
https://doi.org/10.1029/2009JB000820, 2010.

Tanguy, J. C., Condomines, M., Branca, S., La Delfa, S., and Coltelli, M.: New archeomagnetic and 226Ra-230Th dating of recent lavas for the Geological map of Etna volcano. Italian Journal of Geosciences, 131(2), 241-257, https://doi.org/10.3301/IJG.2012.01, 2012.

825 Tibaldi, A., Bonali, F.B., Corti, N., Russo, E., Drymoni, K., De Beni, E., Branca, S., Neri, M., Cantarero, M. and Pasquarè Mariotto, F.: Surface deformation during the 1928 fissure eruption of Mt Etna (Italy): insights from field data and FEM numerical modelling, Tectonophysics, 837, 229468, https://doi.org/10.1016/j.tecto.2022.229468, 2022.

Tibaldi, A., Corti, N., De Beni, E., Bonali, F.B., Falsaperla, S., Langer, H., Neri, M., Cantarero, M., Reitano, D., Fallati, L.: Mapping and evaluating kinematics and the stress and strain field at active faults and fissures: a comparison between field and

830 drone data at the NE rift, Mt Etna (Italy), Solid Earth, 12, 801–816, https://doi.org/10.5194/se-12-801-2021, 2021.

Tibaldi, A. and Groppelli, G.: Volcano-tectonic activity along structures of the unstable NE flank of Mt. Etna (Italy) and their possible origin, J. of Volcanology and Geothermal Research, 115, 277–302, https://doi.org/10.1016/S0377-0273(01)00305-5, 2002.

Tringali, G.: Earthquake surface faulting and aseismic creep on Etna volcano: role of the pre-volcanic basement, relationships

835 with flank instability and magmatic intrusions, implications for future hazard scenarios, Ph.D. thesis, Università degli Studi dell'Insubria, Italy, https://hdl.handle.net/11383/2165092, 2023.

Tringali, G., Bella, D., Livio, F. A., Ferrario, M.F., Groppelli, G., Blumetti, A. M., Di Manna, P., Vittori, E., Guerrieri, L., Porfido, S., Boso, D., Pettinato, R., Paradiso, G., and Michetti, A. M.: Fault rupture and aseismic creep accompanying the December 26, 2018, Mw 4.9 Fleri earthquake (Mt. Etna, Italy): Factors affecting the surface faulting in a volcano-tectonic

840 environment, Quaternary International, 651, 25-41, https://doi.org/10.1016/j.quaint.2021.12.019, 2023a.

Tringali, G., Bella, D., Livio, F., Ferrario, M. F., Groppelli, G., Pettinato, R., and Michetti, A. M.: Aseismic creep and gravitational sliding on the lower eastern flank of Mt. Etna: Insights from the 2002 and 2022 fault rupture events between Santa Venerina and Santa Tecla, Tectonophysics, 856, 229829, https://doi.org/10.1016/j.tecto.2023.229829, 2023b.

Urlaub, M., Petersen, F., Gross, F., Bonforte, A., Puglisi, G., Guglielmino, F., Krastel, S., Lange, D., and Kopp, H.:

845 Gravitational collapse of Mount Etna's southeastern flank, Science Advances, 4(10), eaat9700, https://doi.org/10.1126/sciadv.aat9700, 2018.

Walter, T. R., Acocella, V., Neri, M., and Amelung, F.: Feedback processes between magmatic events and flank movement at Mount Etna (Italy) during the 2002–2003 eruption, J. of Geophysical Research: Solid Earth, 110(B10), https://doi.org/10.1029/2005JB003688, 2005a.

850 Walter, T. R., Troll, V. R., Cailleau, B., Belousov, A., Schmincke, H. U., Amelung, F., and Vd Bogaard, P.: Rift zone reorganization through flank instability in ocean island volcanoes: an example from Tenerife, Canary Islands, Bulletin of Volcanology, 67, 281-291, https://doi.org/10.1007/s00445-004-0352-z, 2005b.

Walter, T. R., and Troll, V. R.: Experiments on rift zone evolution in unstable volcanic edifices, J. of Volcanology and Geothermal Research, 127(1-2), 107-120, https://doi.org/10.1016/S0377-0273(03)00181-1, 2003.